

# In situ Cosmogenic $^{10}\text{Be}$ and $^{26}\text{Al}$ Reveal a Complex Exposure and Erosion History of the Landscape Once Covered by the Quebec-Labrador Ice Dome

Peyton M. Cavnar<sup>1,2</sup>, Paul R. Bierman<sup>1,2</sup>, Jeremy D. Shakun<sup>3</sup>, Lee B. Corbett<sup>1</sup>, Danielle LeBlanc<sup>3</sup>, Gillian L. Galford<sup>1,2</sup>, Pierre-Olivier Couette<sup>4,5</sup>, Jean-Francois Ghienne<sup>5</sup>, Patrick Lajeunesse<sup>4</sup>, Jérôme van der Woerd<sup>5</sup>, and Marc Caffee<sup>6</sup>

<sup>1</sup>Rubenstein School for the Environment and Natural Resources, University of Vermont, Burlington, United States

<sup>2</sup>Gund Institute for the Environment, Burlington, United States

<sup>3</sup>Department of Earth and Environmental Sciences, Boston College, Chestnut Hill, 02467, United States

<sup>4</sup>Département de Géographie, Université Laval, Québec, Canada

<sup>5</sup>Institut Terre & Environnement de Strasbourg (ITES), UMR 7063, CNRS, Université de Strasbourg, Strasbourg, France

<sup>6</sup>PRIME Laboratory, Purdue University, West Lafayette, 47907, United States

<sup>3,7</sup>Woods Hole Oceanographic Institution, Falmouth, MA, United States

*Correspondence to:* Peyton M. Cavnar ([cavnar.peyton@gmail.com](mailto:cavnar.peyton@gmail.com)) and Paul Bierman ([pbierman@uvm.edu](mailto:pbierman@uvm.edu))

**Abstract.** The rate at which ice sheets erode rock to produce sediment is poorly known. Here, we use paired cosmogenic nuclides in both deglacial and modern sediment to understand better the efficacy with which the Quebec-Labrador Ice Dome (QLID) of the Laurentide Ice Sheet eroded bedrock to generate sand and boulders across the landscape of eastern Canada. We sampled deglacial esker and delta sand ( $n = 10$ ), sediment from 11 modern streams, and a bedrock outcrop and depth profile, measuring concentrations of  $^{10}\text{Be}$  and  $^{26}\text{Al}$  in quartz isolated from all samples. We also collated published cosmogenic nuclide measurements of boulders and bedrock from eastern Canada ( $n = 238$  samples) and using estimates of deglaciation timing, calculated nuclide concentrations when the material was exposed by the most recent deglaciation, between 6.3 to 15.2 ka.

At the time of deposition, all 10 deglacial sand samples contained  $^{10}\text{Be}$  and  $^{26}\text{Al}$ , equivalent on average to several thousand years of surface exposure. The ubiquitous presence of  $^{10}\text{Be}$  and  $^{26}\text{Al}$  in eastern Quebec deglacial sediment is consistent with commonly older-than-expected exposure ages for bedrock outcrops ( $n = 26$  of 46 samples) and boulders ( $n = 65$  of 192 samples) once covered by the QLID. Error-weighted averages of  $^{26}\text{Al}/^{10}\text{Be}$  ratios for both deglacial ( $6.1 \pm 1.2$ , all uncertainties 1 SD) and modern sediment samples ( $6.6 \pm 0.5$ ) are lower than the measured production ratio at high latitudes ( $7.3 \pm 0.3$ ), suggesting cumulative burial of at least some sediment grains for at least hundreds of thousands of years.

Such burial suggests that ice at the center of the QLID either survived some interglacials and/or that the average sediment residence time on the landscape is several times longer than a 100 ky glacial cycle, allowing repeated storage and burial of sediment, over multiple glacial cycles, both under ice and in thick deposits such as deltas and moraines. Modern river sand contains on average only slightly higher nuclide concentrations than deglacial sediments, suggesting that river sand is predominately recycled from glacial deposits. Together, these data suggest that the depth of bedrock erosion by ice and the speed of glacial sediment transport in eastern Canada were

insufficient to remove material containing cosmogenic nuclides produced during prior interglacial(s) from at least some bedrock outcrops and boulders, and from all glacially transported sediment that we sampled.

## 1. Introduction

Ice sheets are important geomorphic agents of high-latitude landscape change (Patton et al., 2024; Sugden, 1978; Wilner et al., 2024) although the rates at which they erode landscapes and transport sediment are not well quantified. Data suggest that both erosion and sediment transport rates are spatially and temporally variable (e.g., Alley et al., 2019; Cowton et al., 2012; Hallet et al., 1996; Patton et al., 2022). Rates of glacial erosion appear to be sensitive to time-scale bias, making it difficult to accurately compare short-term, contemporary rates of glacial erosion and sediment export to those determined over longer time scales (Ganti et al., 2016; Wilner et al., 2024). Modelling sub-glacial processes, including erosion and sediment transport, is not straightforward and results do not always match field evidence (e.g., Hildes et al., 2004).

During the Last Glacial Maximum (LGM), between 20-25 ka, the Laurentide Ice Sheet (LIS) covered most of Canada and the northern United States (Dalton et al., 2022). It was the largest body of ice in the Northern Hemisphere holding about 70 meters of sea level equivalent (Simms et al., 2019). Its ablation during the latest Pleistocene and early Holocene (characterized by collapse of northern Canadian ice domes) exposed a landscape that was once the ice sheet's bed including rocky outcrops shaped by abrasion and plucking and deposits of glacial and post-glacial sediment (Occhietti et al., 2011). This relict landscape is an archive of past glacial and interglacial landscape behavior that can be used to untangle the history of glacial and interglacial landscape change (Bierman et al., 1999; Booth, 1994; Christ et al., 2021; Collins et al., 2024; Schaefer et al., 2016).

Quantitative geochronology techniques, primarily radiocarbon dating of organic material and cosmogenic nuclide exposure dating of bedrock and boulders, has established the post-LGM retreat history of the LIS (Dalton et al., 2023). Paired nuclide burial dating has provided ages for earlier LIS advances (Balco, 2005; Balco and Rovey, 2008, 2010). Analysis of  $^{10}\text{Be}$  and  $^{26}\text{Al}$  in quartz-bearing ice-rafted debris (IRD) has been used to infer that the LIS did not completely melt away during some and perhaps many interglacials of the last million years (LeBlanc et al., 2023). Yet, uncertainties remain because dates from different chronometers do not always match and the concentrations of cosmogenic nuclides at the time of boulder and bedrock exposure and sediment deposition remain poorly constrained (Bierman et al., 1999, 2015; Briner et al., 2016; Halsted et al., 2024; Staiger et al., 2005).

Our study seeks to understand better the erosivity of LIS ice in eastern Canada by measuring and interpreting the concentrations of the cosmogenic nuclides  $^{26}\text{Al}$  and  $^{10}\text{Be}$  in sediment transported by the LIS. To accomplish this goal, we sampled along two transects stretching outward from the former center of the Quebec-Labrador Ice Dome (QLID) at Labrador City: one eastward toward the Atlantic coast at Goose Bay, Labrador, and another southward to the St. Lawrence River near Quebec City (Figures 1 and 2). To provide context for our samples, we compiled published cosmogenic nuclide analyses of bedrock and glacially transported boulders from the QLID and used independent age estimates of deglaciation to estimate nuclide concentration at the time these sample sites were first exposed by LIS retreat.

The new data, and those we compiled, together allow us to constrain better the accuracy of cosmogenic exposure ages calculated for bedrock surfaces and erratic boulders in areas once covered by the QLID. Our work provides additional context for interpreting cosmogenic nuclide measurements made in sand-sized sediment of glacial and interglacial age present in marine sediment cores collected offshore of former and current ice sheets (e.g.,

Bierman et al., 2016; Christ et al., 2020; LeBlanc et al., 2023) as well sub-ice bedrock and sediment (Bierman et al., 2024a; Christ et al., 2021, 2023; Schaefer et al., 2016).

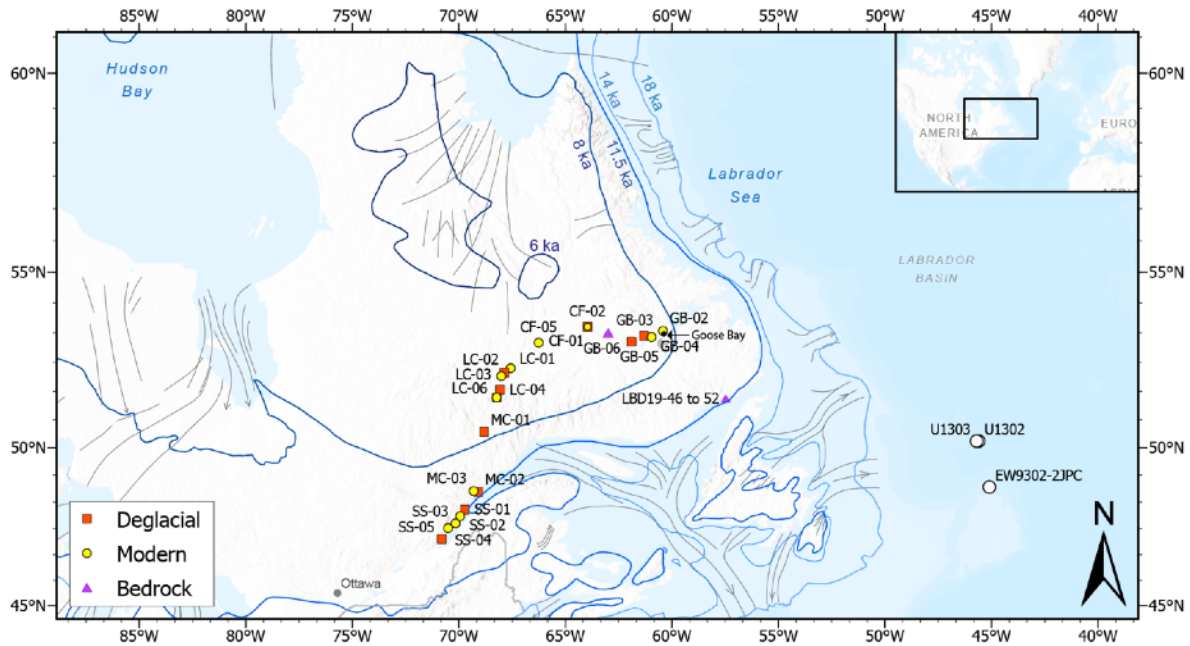


**Figure 1.** Map of field area with sample sites for new data included in this paper. Marine sediment cores with sample analyses in LeBlanc et al. (2023) shown by open circles. Terrestrial samples shown with symbol color and shape corresponding to sample type. Inset indicates location of field area. Grey lines indicate direction of ice flow. Blue deglacial isochrons from Dalton et al. (2020).

## 2. Study Site and Unanswered Questions

The QLID occupied the eastern subarctic Canadian Shield. The area we focus on is underlain mostly by Proterozoic quartzofeldspathic gneisses and granites (Hynes and Rivers, 2010). Regolith and soil are commonly thin (<2.5 m; Pelletier et al., 2016) and punctuated by prominent bedrock outcrops and glacial erratics (Ullman et al., 2016). Central and southern Quebec-Labrador also includes multiple moraine systems that track the final deglaciation of the ice dome into the early Holocene (Couette et al., 2023; Occhietti et al., 2011; Ullman et al., 2016). There are eskers, and substantial ice contact deltas, where the ice front during deglaciation met a body of standing water (Liverman, 1997; Storrar et al., 2013). The paraglacial landscape is still experiencing isostatic glacio-isostatic rebound, with the greatest rebound having occurred near James Bay and southern Hudson Bay (250-270 m; Lajeunesse and Allard, 2005; Lavoie et al., 2012), compared to ~100 m of rebound along coastal eastern Labrador (Andrews and Tyler, 2011).



**Figure 2.** Photographs of representative field sites. A. Modern river sediment at MC-03. B. Deglacial sediment at SS-05. C. Bedrock outcrop at GB-06. D. Deglacial sediment at MC-01. E. Bedrock depth profile at LBD 19 46-52. Depths in cm shown on outcrop. Note sample at 10 cm depth is offset to left of profile.

Notable geographic features in this region include the St. Lawrence River, the Churchill River, and the Manicouagan Reservoir, an annular lake north of the Gulf of St. Lawrence formed in a depression related to an ancient bolide impact (Spray et al., 1998). The St. Lawrence River flows from southwest to northeast and is located

southeast of the QLID's center. The Churchill River flows east from the former center of the Quebec-Labrador Dome, draining into Lake Melville and then the Atlantic Ocean.

Eastern Canada is dominated by boreal spruce forests, sedges, and muskegs (shallow bogs covered in moss), a sub-arctic ecosystem prone to burning during dry periods in the summer, with a recorded fire history stretching back to the 1950's (Payette et al., 1989). Northern Quebec and Labrador are classified under the Dfc climate zone (cool continental climate/subarctic) according to the Koppen climate classification system (Amani et al., 2019; Beck et al., 2018). During winter, ground-based measurements record a mean of ~158 mm of snow water equivalent (SWE) for eastern Canadian boreal forests (Larue et al., 2017).

### 3. Background

#### 3.1. Cosmogenic Nuclides as Recorders of Glacial History and Process

Since the late 1980s, measurement of rare cosmogenic nuclides, most commonly  $^{10}\text{Be}$  and  $^{26}\text{Al}$  extracted from quartz, has helped elucidate the Quaternary history of glaciated landscapes and the rate of glacial processes. Such nuclides are produced by cosmic-ray interaction with target atoms at and near Earth's surface. Near the surface, neutron spallation production is dominant, but deeper in a profile (several meters), muons dominate nuclide production at rates much lower than near the surface (c.f. Braucher et al., 2013).

$^{10}\text{Be}$  and  $^{26}\text{Al}$  are produced in both rock and glacially deposited sediment. Analysis of their concentrations provides information about the timing of deglaciation (e.g., Corbett et al., 2011), the depth of glacial erosion (e.g., Briner et al., 2006; Miller et al., 2006; Stroeven et al., 2002), the persistence of glacial sediment on the landscape (e.g., Nelson et al., 2014), the thermal conditions at the bed (e.g., Staiger et al., 2006), and in the right setting, the limits on the extent and timing of sediment and rock burial by ice sheets (e.g., Bierman et al., 1999; Briner et al., 2006; Christ et al., 2021; Corbett et al., 2016b, c; Marsella et al., 2000; Miller et al., 2006; Schaefer et al., 2016). Measuring the concentrations of  $^{10}\text{Be}$  and  $^{26}\text{Al}$  in the same sample can reveal of periods of burial after surface exposure (Klein et al., 1986) because the nuclides decay at different rates; their half-lives differ by a factor of two (~1.36 and ~0.73 My, respectively).

Cosmogenic nuclide measurements made in detrital sediment from contemporary paraglacial channels (Nelson et al., 2014) and glacial deposits (e.g., Bierman et al., 2016; Goehring et al., 2010), have been used to infer the concentration of nuclides inherited from prior periods of exposure, to interpret ice sheet basal processes (Corbett et al., 2021), and to infer sediment sourcing (e.g., Balco, 2005; Bierman et al., 2016; Fame et al., 2018; Nelson et al., 2014). Cosmogenic nuclide measurements in marine sediments and in material collected from the base of ice cores allow inference of both glacial process and ice sheet history (Bierman et al., 2016, 2024a; Blard et al., 2023; Christ et al., 2020, 2021, 2023; Schaefer et al., 2016; Shakun et al., 2018).

When a landscape is covered by a thick layer of ice such as the LIS, or if sediment is stored in deposits deep enough to prevent most cosmic-ray penetration, production of *in situ*  $^{26}\text{Al}$  and  $^{10}\text{Be}$  slows or stops. As nuclides produced during initial exposure decay, the  $^{26}\text{Al}/^{10}\text{Be}$  ratio decreases (Bierman et al., 1999), a change that is detectable after several hundred thousand years of burial (Granger, 2014; Granger and Muzikar, 2001). Re-exposure to cosmic rays at or near Earth's surface increases the  $^{26}\text{Al}/^{10}\text{Be}$  ratio and in time it approaches the production ratio. However, if sediment remains buried meters below the surface during interglacial periods (such as in deglacial

deltas, till sheets, and eskers or under ice),  $^{26}\text{Al}$  and  $^{10}\text{Be}$  concentrations and the  $^{26}\text{Al}/^{10}\text{Be}$  at the time of deposition are preserved in whole (deep burial) or in part (shallow burial) (Bierman et al., 2016; Goehring et al., 2010; Nelson et al., 2014).

Concentrations of  $^{10}\text{Be}$  and  $^{26}\text{Al}$  in glacial sediment therefore reflect the convolved history of that sediment and of the ice sheet that eroded and transported it over time (e.g., Bierman et al., 2016; Briner et al., 2016; Corbett et al., 2021; Goehring et al., 2010; Nelson et al., 2014). Analysis of sediment deposited by retreating ice sheets allows inferences about erosion and transport efficiency at and near the former or present ice sheet bed. Long interglacial exposures, thin sediment cover, and bedrock that is resistant to erosion will allow high concentrations of nuclides to accumulate – for example, in central North America (Balco, 2005). On the other hand, persistent ice cover, high rates and depths of glacial erosion, and efficient sediment transport by ice will lower nuclide concentrations in glacially derived sediment, such as in southern and western Greenland (Goehring et al., 2010; Nelson et al., 2014).

### **3.2. Uncertain Laurentide Ice Sheet History in Eastern Canada**

For most of the last glaciation, the LIS was characterized by three major ice domes, regions of especially thick (~4 km in some places), outflowing ice: Foxe Baffin Dome, Keewatin Dome, and the QLID considered here (Stokes et al., 2012). Changes in LIS size are thought to have broadly tracked the marine oxygen isotope record, though uncertainties in ice volume and extent through time reflect the paucity of geologic constraints (Batchelor et al., 2019).

The extent and duration of ice cover in eastern Canada during the Pleistocene remains uncertain. For example, the majority of Canada may have been ice-covered, with the LIS reaching 70% of its LGM extent as early as Marine Isotope Stage (MIS) 5d (~110 ka) or not until MIS 4 (~60 ka) (Dalton et al., 2022). During subsequent retreat into MIS 3 (~45 ka), a combination of luminescence,  $^{14}\text{C}$ , and cosmogenic nuclide ( $^{10}\text{Be}$  and  $^{26}\text{Al}$ ) dating, along with evidence of a marine incursion into Hudson Bay, were used to argue for deglaciation of the center of the LIS there (Dalton et al., 2019; Pico et al., 2018). Others disagreed, interpreting these ages differently and citing the timing of carbonate-rich Heinrich events H5 and H4 which indicate that an intact Hudson Strait ice stream existed during MIS 3 (Gauthier et al., 2024; Hodder et al., 2023, 2024; Miller and Andrews, 2019). Recent measurements of cosmogenic nuclide concentrations in quartz-bearing ice rafted debris (IRD), sourced at least in part from LIS-generated icebergs, also suggest ice may have lingered in eastern Canada through many interglacial periods (LeBlanc et al., 2023). Evidence includes  $^{26}\text{Al}/^{10}\text{Be}$  ratios ( $4.7 \pm 0.8$ ) well below the high-latitude production value of  $7.3 \pm 0.3$  (Corbett et al., 2017). Such depressed ratios require long (>1 My) periods of burial (by ice, sediment, or water) throughout the Pleistocene.

Retreat of the LIS in Quebec and Labrador following the LGM is constrained by radiocarbon ages on post-glacial marine shells and lake organic material (Dalton et al., 2020; Dyke, 2004). These data suggest that the initial retreat was gradual, with the eastern margin pulling back slowly from the continental shelf and not reaching the modern coastline until ~11.5 ka (Figure 1). Retreat rate increased when the Hudson Bay opened and the QLID separated from other sectors of the LIS after ~8.5 ka. The margin of the then retreated rapidly toward the center of the landmass, disappearing entirely by ~6 ka.

In situ produced cosmogenic nuclides have been used extensively to date retreat of the QLID after the LGM in Labrador and Quebec. Clark et al. (2003) report 27 measurements (including 2 replicates) of  $^{10}\text{Be}$  on 21 boulders and 4 bedrock surfaces, concluding that ice left valleys in the Torngat Mountains of northeastern Labrador

between 12.0 and 13.4 ka. Further south, Ullman et al. (2016) used  $^{10}\text{Be}$  concentrations in 65 boulder samples to demonstrate that ice left eastern Labrador at 10.4 ka and the St. Lawrence coastline in southern Quebec at 9.2 ka, reaching the center of the Quebec-Labrador landmass at 6.7 ka. Couette et al. (2023) interpreted 37  $^{10}\text{Be}$  exposure ages on boulders to represent five still-stands or re-advances of the eastern LIS margin as it retreated inland from the coast of eastern Labrador (~12.9 ka, ~11.5 ka, ~10.4 ka, ~9.3 ka, and ~8.4-8.2 ka). Carlson et al. (2007), using 13 boulder measurements, determined that deglaciation across central Quebec occurred rapidly between 8.0 and 6.8 ka. Along western Ungava Bay, Lefebvre–Fortier et al., (2024) obtained  $^{10}\text{Be}$  ages on 14 boulders from five marine strandlines, which suggest north-to-south ice margin retreat from 8.9 to 7.9 ka. Dubé-Loubert et al. (2018, 2021) placed deglaciation between 8.6 and 8.0 ka south of Ungava Bay based on 30 boulder ages from glaciomarine and ice-dammed lake delta surfaces. In the same region of northeastern Labrador, Rice et al. (2019)  $^{10}\text{Be}$  dated 8 bedrock and 2 boulder samples. Rejecting two much older ages, they report a range of ages from 9.8 to 6.2 ka.

Taken together, the cosmogenic data generally agree with Dalton et al.'s (2020) radiocarbon-based chronology of deglaciation in eastern Canada. The  $^{10}\text{Be}$  ages show a pattern of radial ice margin retreat toward the center of Quebec-Labrador. However, many of the cosmogenic nuclide studies in this region of eastern Canada (Clark et al., 2003; Couette et al., 2023; Dubé-Loubert et al., 2018, 2021; Marquette et al., 2004; Rice et al., 2019) identify older-than-expected  $^{10}\text{Be}$  ages, which they attribute to inheritance of cosmogenic nuclides from periods of prior exposure. Ullman et al. (2016) note that radiocarbon ages lag the  $^{10}\text{Be}$  ages along their transects across the western, eastern, and southern part of the former QLID by centuries. This discrepancy could represent the pervasive presence of inherited nuclides – albeit a low concentration - inherited from an earlier near-surface exposure or a lag in revegetation after deglaciation (c.f., Halsted et al., 2024).

### 3.3. Assessing the Erosivity of Ice Sheets

In some places, ice sheets erode their bed (Alley et al., 2019; Cowton et al., 2012) and in others, they preserve bed materials (Bierman et al., 2024b). Erosion is considered typical of warm-based ice, whereas bed preservation is thought common where ice is cold-based and frozen to the bed (e.g., Corbett et al., 2016b; Sugden, 1978). Data generally support these assumptions (Koppes et al., 2015), although stratigraphic observations clearly show that ice, both warm and cold-based, can leave older sediment outcrops intact. For example, field surveys in areas overrun by the LIS reveal weathered regolith (Goldthwait and Kruger, 1938) including the fossiliferous Eocene Brandon Lignite (Tiffney, 1994) in valleys where ice was warm-based, meaning that pre-glacial, poorly consolidated material has survived repeated LIS advances in New England, south of the field area investigated here. Weathered saprolite is similarly preserved in southeastern Quebec (LaSalle et al., 1985). On Baffin Island, pre-LGM lake sediments remain in basins overrun by ice as does heavily weathered bedrock on which sit fresh, late-glacial erratic boulders (Bierman et al., 2001).

Others have found varying inheritance of cosmogenic nuclides in boulders and bedrock sampled near and inside the former LGM margin of the LIS. They attributed higher-than-expected nuclide concentrations to boulder reworking and insufficiently deep surface erosion during the brief time the ice occupied areas near the ice margin (Balco et al., 2002; Balter-Kennedy et al., 2024; Barth et al., 2019; Colgan et al., 2002; Halsted et al., 2024). In the northeastern United States, Halsted et al. (2024) estimated that boulders on LIS terminal moraines contained concentrations of inherited  $^{10}\text{Be}$  equivalent to 2-6 ka of surface exposure. Mountain summits in New England, which

till deposits indicate were covered by LGM ice, also have samples with much higher than expected cosmogenic exposure ages (Bierman et al., 2015; Corbett et al., 2019; Davis et al., 2015; Koester et al., 2021). In south-central Wisconsin, near the LGM ice margin, three out of five bedrock outcrops sampled had concentrations of  $^{10}\text{Be}$  and  $^{26}\text{Al}$  many times higher than predicted based on radiocarbon dating (Colgan et al., 2002). In the Torngat Mountains of northern Labrador, measurements of  $^{26}\text{Al}$  and  $^{10}\text{Be}$  on bedrock sites and erratic boulders at mountain summits provide evidence of minimal erosion ( $<1.4 \text{ m Ma}^{-1}$ ) and thus large concentrations of inherited nuclides where cold-based ice was predominant before deglaciation (Staiger et al., 2005).

Significant inheritance of cosmogenic nuclides is observed in areas once occupied by other Northern Hemisphere ice sheets as well. Towards the center of the Scandinavian ice sheet (northeastern Sweden) there is evidence that bedrock outcrops and boulder fields have been preserved through many glacial cycles since the late Cenozoic (Stroeven et al., 2002). There is also evidence of minimal erosion near the margin of the Cordilleran Ice Sheet, with 8 out of 23 bedrock samples on Whitbey Island having  $^{36}\text{Cl}/\text{Cl}$  ratios suggesting inheritance of nuclides produced from prior interglacials (Briner and Swanson, 1998). In northwest Greenland, 8 of 28 sampled boulders had high concentrations of  $^{10}\text{Be}$  and  $^{26}\text{Al}$  along with low  $^{26}\text{Al}/^{10}\text{Be}$  ratios indicative of burial, indicating minimal subglacial erosion over multiple interglacial and glacial periods when the ice was presumably cold-based (Corbett et al., 2016b). Along Greenland's western ice margin, most subglacial cobbles (72 out of 86) sampled by Corbett et al. (2021) had a low concentration of  $^{10}\text{Be}$  (median =  $1.0 \times 10^3 \text{ atoms g}^{-1}$ ), indicative of deep subglacial erosion and/or minimal prior surface exposure. Nevertheless, a subset of samples had higher  $^{10}\text{Be}$  concentrations ( $> 3 \times 10^3 \text{ atoms g}^{-1}$ ,  $n = 14$ ), suggesting sourcing from minimally eroded (cold-based?) regions of the ice sheet where bedrock and sediment retained some  $^{10}\text{Be}$  produced during prior ice-free periods.

Previously-published cosmogenic nuclide concentrations measured in samples of bedrock, boulders, and sediment from the area covered by the QLID suggest a varied pattern of erosion. Some areas were deeply eroded while others show evidence for inherited  $^{10}\text{Be}$  indicating insufficient subglacial erosion to eliminate near-surface-produced cosmogenic nuclides. For example, of the five boulders sampled by Couette et al. (2023) from the early Holocene Paradise Moraine in eastern Labrador, two have implausible  $^{10}\text{Be}$  exposure ages  $>20 \text{ ka}$  and the other three implausibly date the Paradise Moraine as older than a margin further from the center of the ice dome. Ullman et al. (2016) likewise found anomalously high  $^{10}\text{Be}$  concentrations in 10 out of 65 boulders along transects stretching eastward and southward from the center of the Quebec-Labrador Dome to the coast. Marquette et al. (2004) sampled upland bedrock, felsenmeer, and erratics in the Torngat Mountains and analyzed both  $^{26}\text{Al}$  and  $^{10}\text{Be}$ , the concentrations of which suggested that non-erosive ice covered the highlands while erosive ice occupied the valleys, retreating between 11.6 and 13.6 ka. Rice et al. (2019) inferred variable erosion conditions across an  $\sim 100\text{-km}$  portion of northeastern Quebec based on factor-of-two variations in  $^{10}\text{Be}$  abundances of bedrock and till samples. Only Carlson et al. (2007), who collected a 13-sample transect of boulders along a 650 km transect westward from Labrador to James Bay, found no significant inheritance.

### 3.4. Cosmogenic nuclides as sediment source tracers

Cosmogenic nuclides have been used to identify sediment sources for both modern and paleo ice sheets. For example, Nelson et al. (2014) sampled rivers in the deglaciated areas of coastal Greenland. They found  $^{10}\text{Be}$  concentrations in sediment sourced from the ice sheet ( $6,500 \pm 4,100 \text{ atoms g}^{-1}$ ) were significantly lower than sediment sourced from deglaciated terrain ( $14,900 \pm 8,600 \text{ atoms g}^{-1}$ ). This difference can be explained by contrasting

exposure histories. Outboard of the ice margin,  $^{10}\text{Be}$  concentrations in sediment had increased when exposed to cosmic radiation since Holocene deglaciation while concentrations remained low under the ice sheet where production of  $^{10}\text{Be}$  was minimal. Nelson et al. found that sediment sourced from a mix of deglaciated and glaciated terrain had  $^{10}\text{Be}$  concentrations much closer to those of the glacial than deglacial endmember. These results suggest that most sediment moving through river systems in Greenland's paraglacial landscape comes from under the ice sheet rather than the adjacent deglaciated terrain. In southwest Minnesota and eastern South Dakota, Balco (2005) used a similar approach to determine sediment sourcing in a part of the midwestern United States previously covered by the LIS. Rivers there carried sediment with  $^{10}\text{Be}$  and  $^{26}\text{Al}$  concentrations ( $\sim 60,000$  and  $270,000$  atoms  $\text{g}^{-1}$ , respectively) like that of the glacial sediment they sampled. Both materials had lower than production  $^{26}\text{Al}/^{10}\text{Be}$  ( $4.70 \pm 0.29$ ).

## 4. Methods & Materials

### 4.1 Field Methods

We collected deglacial sediment from clean faces in gravel pits or along river bluffs from 2 to 30 m below the upper land surface to reduce the effect of Holocene nuclide production following deglaciation (Table 2). We used shovels to dig  $\sim 0.3$  m into the side of the landform before collecting  $\sim 500$  g of sand. Modern river sediment samples were collected along channels away from areas of recent disturbance. We collected outcrop samples using a rock saw and chisels. The single sample is from an exposed outcrop on a glacially molded bedrock knob in the middle of our eastern transect. This sample is close to Ullman et al. (2016) site CL3, in which two of five boulders they sampled contained what the authors interpreted as inherited nuclides from period(s) of prior near-surface exposure. The coastal location is a roadcut 4 km inboard of the Belles Amours Moraine at the northern tip of the Gulf of St. Lawrence, where we obtained 7 samples along a 1.9 m bedrock depth profile; the surface sample (LBD19-46) was reported previously by Couette et al. (2023).

To constrain nuclide concentrations in materials deposited by the LIS, we sampled deglacial sediment deposits ( $n=10$ ) including deltas and eskers. We collected modern river sediment samples ( $n=11$ ) from trunk streams (St. Lawrence and Churchill River) as well as smaller tributaries.

**Table 1. Sample Location and Type**

Sample Name	Type	Latitude <sup>a</sup>	Longitude <sup>a</sup>	Elevation (m) <sup>a</sup>
CF-02	Glacial Delta	53.5077	-63.9545	167
LC-02	Esker	52.2011	-67.8722	537
LC-04	Ice Contact Fan	51.7102	-68.0719	440
LC-05	Ice Contact Fan	51.4881	-68.2192	391
MC-01	Esker	50.4748	-68.8101	500
MC-02	Glacial Delta	48.6452	-69.0854	10
GB-03	Glacial Delta	53.2572	-60.7848	36

GB-05	Esker	53.0922	-61.8920	402
SS-01	Glacial Delta	48.1030	-69.7213	10
SS-05	Glacial Delta	47.1669	-70.8047	307
CF-01	Modern River Sediment	53.5060	-63.9585	126
CF-05	Modern River Sediment	53.0595	-66.2555	527
LC-01	Modern River Sediment	52.3365	-67.5671	533
LC-03	Modern River Sediment	52.1107	-68.0073	645
LC-06	Modern River Sediment	51.4882	-68.2229	401
GB-02	Modern River Sediment	53.3934	-60.4229	2
GB-04	Modern River Sediment	53.2201	-60.9549	210
MC-03	Modern River Sediment	48.6779	-69.3045	61
SS-02	Modern River Sediment	47.8942	-69.9368	128
SS-03	Modern River Sediment	47.6665	-70.1589	3
SS-04	Modern River Sediment	47.5157	-70.5066	25
GB-06	Bedrock	53.3351	-62.9912	484
LBD19-46 to LBD19-52	Bedrock Depth Profile	51.4780	-57.4756	75

<sup>a</sup> Location and elevation were measured in the field using a Garmin eTrex 20 GPS

## 4.2 Laboratory Methods

### 4.2.1 University of Vermont

To isolate and purify quartz for cosmogenic nuclide analysis at the University of Vermont (all sediment samples and the surface bedrock sample) we used a series of physical and chemical processes (Kohl and Nishiizumi, 1992) after sieving material to between 250 and 850  $\mu\text{m}$ . We performed two 24-hour 6 N hydrochloric acid etches in heated ultrasonic baths to remove grain coatings. We then used dilute (1%) hydrofluoric and nitric acid etches for three 24-hour periods after which we sonicated samples in 0.5% HF and  $\text{HNO}_3$  for a minimum of two weeks. We evaluated the purity of etched samples using inductively coupled plasma spectrometry optical emission (ICP-OES) after which impure samples were re-etched until each was sufficiently pure.

We extracted beryllium and aluminum from the purified quartz samples (17.3 –22.2 g, n=22) in the National Science Foundation/University of Vermont Community Cosmogenic Facility using methods described in Corbett et al. (2016a). Samples were prepared in two separate batches, each of which included a fully processed blank. We spiked the samples with ~250  $\mu\text{g}$   $^9\text{Be}$  using a beryl carrier made in the Community Cosmogenic Facility with a Be concentration of 348  $\mu\text{g mL}^{-1}$  (Table 4a). We spiked samples with SPEX ICP Al standard (1000 ppm) as needed based on their quantity of native Al, ensuring at least 1500  $\mu\text{g}$  of total Al in every sample.

We quantified total Al in the samples by ICP-OES immediately following sample digestion. Following standard procedures (Corbett et al., 2016a), we removed replicate aliquots from the samples by mass (representing ~2% and ~4% of the sample, respectively), added 25  $\mu\text{L}$   $\text{H}_2\text{SO}_4$  to each, evaporated the HF, then diluted the residual

H<sub>2</sub>SO<sub>4</sub> droplets by mass with a 0.25% H<sub>2</sub>SO<sub>4</sub> solution spiked with Y as an internal standard. Purdue Rare Isotope Measurement Laboratory performed accelerator mass spectrometry analysis (AMS). For <sup>10</sup>Be/<sup>9</sup>Be, measured ratios were normalized to primary standard 07KNSTD3110 with a ratio of  $2850 \times 10^{-15}$  (Nishiizumi et al., 2007). For <sup>26</sup>Al/<sup>27</sup>Al, analyses were normalized to primary standard KNSTD with a ratio of  $1.818 \times 10^{-12}$  (Nishiizumi, 2004).

We used the known concentration of <sup>9</sup>Be added as carrier, along with the measured isotopic ratio and quartz mass, to calculate the concentration of <sup>10</sup>Be in each sample. Because of the native <sup>27</sup>Al within the samples, the concentration of <sup>27</sup>Al measured using ICP-OES after quartz dissolution was used to calculate the concentration of <sup>26</sup>Al. We subtracted the mean extraction process blank ratios of <sup>10</sup>Be/<sup>9</sup>Be ( $(7.41 \pm 2.81) \times 10^{-16}$ ; n = 2) and <sup>26</sup>Al/<sup>27</sup>Al ( $(5.39 \pm 0.71) \times 10^{-16}$ ; n = 2) from the measured ratios and propagated the uncertainty in quadrature (Tables 3 and 4).

#### 4.2.2 University of Strasbourg

To isolate and purify quartz for cosmogenic nuclide analysis at the University of Strasbourg, Institut Terre et Environnement de Strasbourg (7 bedrock profile samples, LBD19-46 to 52) we used a series of physical and chemical processes (Bierman et al., 2002; Kohl and Nishiizumi, 1992). We sieved material to between 250 and 1000 μm. For each sample, we performed a 12-hour 6 N hydrochloric acid (HCl) leaching to eliminate oxides and organic material. Magnetic minerals were then separated with a Frantz magnetic separator. We used dilute (1%) hydrofluoric (HF) and nitric (HNO<sub>3</sub>) acid etches in ultrasonic baths for five 12-hour periods. We evaluated the purity of etched samples using inductively coupled plasma optical emission spectroscopy (ICP-OES) after which impure samples were re-etched until each was sufficiently pure.

We extracted beryllium and aluminum from the purified quartz samples (27.02 – 56.99 g, n = 7) in the cosmogenic nuclide laboratory at the University of Strasbourg following a protocol modified from Kohl and Nishiizumi (1992). Samples were prepared together with a fully processed blank. We spiked the samples with ~250 or ~500 μg <sup>9</sup>Be using a Scharlab ICP 1000 mg/l Be standard. We spiked only the blank with a Scharlab ICP 1000 mg/l Al standard as the quantity of native Al was sufficient in every sample.

We quantified total Al in the samples by ICP-OES following sample digestion and three successive fuming steps with 2 to 4 ml of perchloric acid (HClO<sub>4</sub>). Beryllium and aluminum were isolated through anion and cation exchange columns and precipitated as hydroxides. They were then dried and calcinated to BeO and Al<sub>2</sub>O<sub>3</sub> at 750°C. AMS analysis was performed at ASTER, the French National Laboratory of Cosmogenic Nuclides in CEREGE (Aix-en-Provence). For <sup>10</sup>Be/<sup>9</sup>Be, measured ratios were normalized to in-house CEREGE standard STD-11 with an assumed ratio of  $(1.191 \pm 0.013) \times 10^{-11}$  (Braucher et al., 2015). For <sup>26</sup>Al/<sup>27</sup>Al, analyses were normalized to in-house CEREGE standard SM-AL-11 with a ratio of  $(7.401 \pm 0.064) \times 10^{-12}$  (Merchel and Bremser, 2004).

We used the known concentration of <sup>9</sup>Be added as carrier, along with the measured isotopic ratio and quartz mass to calculate the concentration of <sup>10</sup>Be in each sample. Because of the native <sup>27</sup>Al within the samples, the concentration of <sup>27</sup>Al measured using ICP-OES after quartz dissolution was used to calculate the concentration of <sup>26</sup>Al. We subtracted the extraction process blank ratios of <sup>10</sup>Be/<sup>9</sup>Be ( $(5.21 \pm 0.42) \times 10^{-15}$ ) and <sup>26</sup>Al/<sup>27</sup>Al ( $(6.25 \pm 6.25) \times 10^{-16}$ ) from the measured ratios and propagated the uncertainty in quadrature.

#### 4.3 Statistical Analysis

We use the same value ( $\alpha = 0.05$ ) for all statistical tests we perform. We used both Wilcoxon rank-sum tests (due to the non-normal distribution of nuclide concentrations in modern sediment samples) and Tukey HSD tests to investigate significant differences between sample groups. We used a 2-standard deviation threshold for detectability; that is, if twice the analytical uncertainty exceeded the measured ratio, then we considered the sample to be below detection limits. This provides a 95% confidence that the isotopic ratios and concentrations we report are finite.

#### 4.4 Data Compilation

To expand our assessment of cosmogenic nuclide concentrations in materials influenced by the QLID, we estimated the concentration of inherited nuclides present in published  $^{10}\text{Be}$  data generated from samples of boulders and bedrock collected in the region by others. We obtained data from 200 samples (42 bedrock, 158 boulders) from Dalton et al.'s, (2023) North American  $^{10}\text{Be}$  compilation and recalculated all ages with an online exposure calculator (Balco et al., 2008) using the global production rate and LSDn scaling (Lifton et al., 2014), accounting for differences in standardizations. We also included 37  $^{10}\text{Be}$  ages (3 bedrock, 34 boulders) from Couette et al. (2023) that were not in the Dalton et al. (2023) compilation, following the same protocol.

#### 4.5 Holocene Exposure Correction

For deglacial sediment samples and the single inland bedrock sample, we calculated the concentration of nuclides attributable to Holocene exposure. We used the online exposure age calculator formerly known as CRONUS (constant production rate model, version 3.0.2, constants 2020-08-26) to determine the surface production rate (atoms  $\text{g}^{-1} \text{yr}^{-1}$ ) of  $^{10}\text{Be}$  and  $^{26}\text{Al}$  for both muons ( $P_\mu$ ) and spallation ( $P_s$ ) at each sample site (Balco et al., 2008). The production rate at depth was then estimated using an attenuation length of 165  $\text{g cm}^{-2}$  for spallation ( $A_s$ ) and 1400  $\text{g cm}^{-2}$  for muons ( $A_\mu$ ). For sediment, we assumed a density ( $\rho$ ) of 1.7  $\text{g/cm}^3$ . By establishing the nuclide production rate at depth, we calculated (using equation 1) the production since deglaciation ( $A$  in yr) of  $^{10}\text{Be}$  and  $^{26}\text{Al}$  ( $H$  in atoms  $\text{g}^{-1}$ ) at the depth where collected each samples ( $D$  in cm) taking deglaciation age estimates for each sample site from Dalton et al. (2020) using equation 1. For the rock sample, we used zero depth.

$$H = P_s \cdot 1/\exp\left(\frac{D \cdot \rho}{\Lambda_s}\right) \cdot A + P_\mu \cdot 1/\exp\left(\frac{D \cdot \rho}{\Lambda_\mu}\right) \cdot A$$

(1)

We validated the apparent muonogenic attenuation factor using the CRONUS implementation of Heisinger et al., (2002) (code P\_mu\_total.m) for sea level— yielding < 1% difference from our original calculations. We estimated uncertainties in the concentration of nuclides produced during the Holocene due to uncertainties in our sample depths and combined these in quadrature with AMS measurement uncertainties (Table 2).

To correct for postglacial exposure in boulder and bedrock samples, we used deglaciation ages interpolated from the Dalton et al. (2020) radiocarbon-based LIS margin isochrons. The concentration, calculated from this age

convolved with the site-specific production rate, was subtracted from the sample's measured  $^{10}\text{Be}$  concentration to calculate the concentration of inherited nuclides. We did not use the more recent reconstruction of LIS retreat from Dalton et al. (2023) to determine deglaciation ages because it incorporates updates based on the  $^{10}\text{Be}$  data and thus risks circularity. We estimated the amount of inheritance in our coastal bedrock depth profile by fitting a production profile to the data representing 11.5 ky of exposure (the age of the adjacent Belles Amours Moraine; Couette et al., 2023) with varying concentrations of uniformly distributed inherited nuclides.

**Table 2. Calculations for Holocene Exposure-Corrected Concentrations**

Sample Name	Age (yr) <sup>a</sup>	Sample Depth (cm) <sup>b</sup>	Depth Uncertainty (cm) <sup>b</sup>	$^{10}\text{Be}$ Muon Production Rate (atoms $\text{g}^{-1} \text{y}^{-1}$ ) <sup>c</sup>	$^{26}\text{Al}$ Muon Production Rate (atoms $\text{g}^{-1} \text{y}^{-1}$ ) <sup>c</sup>	$^{10}\text{Be}$ Spallation Rate (atoms $\text{g}^{-1} \text{y}^{-1}$ ) <sup>c</sup>	$^{26}\text{Al}$ Spallation Rate (atoms $\text{g}^{-1} \text{y}^{-1}$ ) <sup>c</sup>	Total $^{10}\text{Be}$ production rate at depth (atoms $\text{g}^{-1} \text{y}^{-1}$ ) <sup>d</sup>	Total $^{26}\text{Al}$ production rate at depth (atoms $\text{g}^{-1} \text{y}^{-1}$ ) <sup>d</sup>	$^{10}\text{Be}$ correction (%)
CF-02	800	800	-200, +200	0.193	1.612	5.49	37.05	0.0745	0.6200	3
LC-02	780	250	-50, +50	0.220	1.838	7.80	52.63	0.7559	5.3617	25
LC-04	790	200	-50, +50	0.212	1.774	7.11	47.98	1.0719	7.5030	41
LC-05	770	250	-50, +50	0.209	1.743	6.78	45.76	0.6702	4.7688	19
MC-01	860	180	-30, +20	0.217	1.811	7.49	50.50	1.3468	9.3599	62
MC-02	12400	2000	-200, +200	0.181	1.513	4.54	30.61	0.0160	0.1334	1
GB-03	840	700	-200, +200	0.185	1.540	4.82	32.52	0.0826	0.6822	8
GB-05	830	300	-100, +100	0.211	1.759	6.96	46.94	0.4630	3.3559	18
SS-01	12300	550	-150, +50	0.181	1.511	4.50	30.39	0.1084	0.8800	12
SS-05	12800	3000	-500, +500	0.201	1.681	5.99	40.44	0.0053	0.0440	0
GB-06	810	0	0	0.217	1.811	7.51	50.67	7.727	52.481	85

<sup>a</sup>Deglaciation ages estimated based on proximity to deglacial isochrons in Couette et al. (2023)

<sup>b</sup>Sample depth estimated in the field. Depth uncertainty estimated from photos and considered 95% confidence interval.

<sup>c</sup>Muon and spallation surface production rates estimated from the online calculator formerly known as CRONUS (Balco et al., 2008)

<sup>d</sup>Total nuclide production rate at sample depth includes production from both muons and spallation, and assumes an attenuation length of 165  $\text{g cm}^{-2}$  for spallation and 1400  $\text{g cm}^{-2}$  for muons.

## 5. Results

$^{10}\text{Be}$  and  $^{26}\text{Al}$  were above detection limit in all 8 bedrock samples and 21 of 22 sediment samples we analyzed, the one exception being the  $^{26}\text{Al}$  measurement for sample GB-04, a modern stream sample (Table 3, Figure 3). For both nuclides, the average concentration is higher in the modern sediment ( $3.31 \pm 1.57 \times 10^4$   $^{10}\text{Be}$  atoms  $\text{g}^{-1}$ ,  $2.12 \pm 1.18 \times 10^5$   $^{26}\text{Al}$  atoms  $\text{g}^{-1}$ ) than in the deglacial sediment ( $2.25 \pm 1.30 \times 10^4$   $^{10}\text{Be}$  atoms  $\text{g}^{-1}$ ,  $1.47 \pm 0.94 \times 10^5$   $^{26}\text{Al}$  atoms  $\text{g}^{-1}$ ).

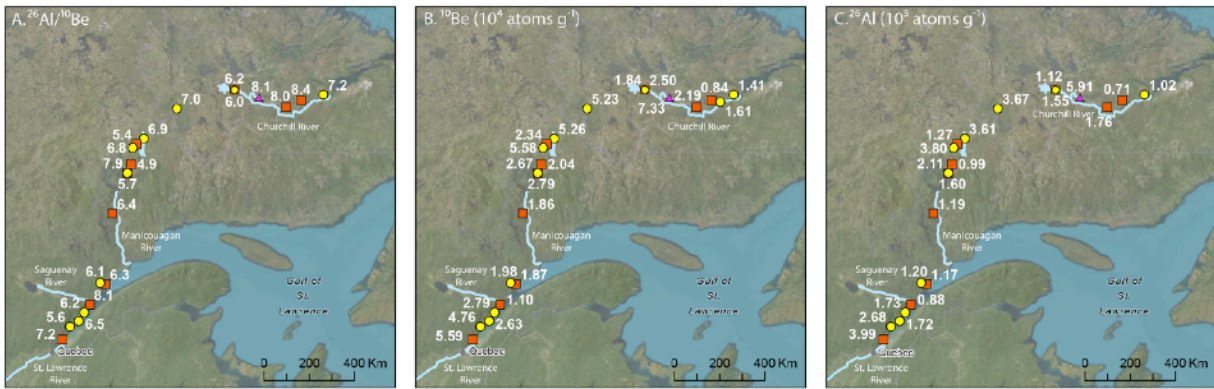


**Figure 3.** Maps showing new isotopic data excluding bedrock depth profile. A.  $^{26}\text{Al}/^{10}\text{Be}$  ratio ( $n=21$ ). B. Measured concentration of  $^{10}\text{Be}$  ( $n=22$ ). C. Measured concentration of  $^{26}\text{Al}$  ( $n=21$ ). Data in Table 3. Sample names and key as in Figure 1.

**Table 3. Blank-corrected Isotopic Data**

Sample Name	Type	$^{10}\text{Be}$ (atoms $\text{g}^{-1}$ )	Uncertainty ( $\text{atoms g}^{-1}$ )	$^{26}\text{Al}$ (atoms $\text{g}^{-1}$ )	Uncertainty ( $\text{atoms g}^{-1}$ )	$^{26}\text{Al}/^{10}\text{Be}$	$^{26}\text{Al}/^{10}\text{Be}$ Uncertainty
CF-02	Deglacial	$1.84 \times 10^4$	$1.30 \times 10^3$	$1.12 \times 10^5$	$1.08 \times 10^4$	6.05	0.72
LC-02	Deglacial	$2.34 \times 10^4$	$1.45 \times 10^3$	$1.27 \times 10^5$	$1.07 \times 10^4$	5.44	0.57
LC-04	Deglacial	$2.10 \times 10^4$	$1.34 \times 10^3$	$9.94 \times 10^4$	$1.02 \times 10^4$	4.89	0.6
LC-05	Deglacial	$2.79 \times 10^4$	$1.88 \times 10^3$	$1.60 \times 10^5$	$1.67 \times 10^4$	5.72	0.71

MC-01	Deglacial	$1.86 \times 10^4$	$1.61 \times 10^3$	$1.19 \times 10^5$	$1.43 \times 10^4$	6.38	0.95
MC-02	Deglacial	$1.87 \times 10^4$	$1.54 \times 10^3$	$1.17 \times 10^5$	$9.56 \times 10^3$	6.27	0.73
GB-03	Deglacial	$8.42 \times 10^3$	$1.68 \times 10^3$	$7.11 \times 10^4$	$3.23 \times 10^4$	8.44	4.19
GB-05	Deglacial	$2.19 \times 10^4$	$1.99 \times 10^3$	$1.76 \times 10^5$	$2.23 \times 10^4$	8.02	1.25
SS-01	Deglacial	$1.10 \times 10^4$	$1.29 \times 10^3$	$8.84 \times 10^4$	$7.98 \times 10^3$	8.05	1.19
SS-05	Deglacial	$5.59 \times 10^4$	$2.63 \times 10^3$	$3.99 \times 10^5$	$2.81 \times 10^4$	7.15	0.61
CF-01	Modern	$2.50 \times 10^4$	$2.17 \times 10^3$	$1.55 \times 10^5$	$1.63 \times 10^4$	6.22	0.85
CF-05	Modern	$5.23 \times 10^4$	$2.18 \times 10^3$	$3.67 \times 10^5$	$2.32 \times 10^4$	7.02	0.53
LC-01	Modern	$5.26 \times 10^4$	$2.33 \times 10^3$	$3.61 \times 10^5$	$1.85 \times 10^4$	6.86	0.47
LC-03	Modern	$5.58 \times 10^4$	$2.41 \times 10^3$	$3.80 \times 10^5$	$2.38 \times 10^4$	6.82	0.52
LC-06	Modern	$2.67 \times 10^4$	$2.12 \times 10^3$	$2.11 \times 10^5$	$1.84 \times 10^4$	7.92	0.93
GB-02	Modern	$1.41 \times 10^4$	$1.41 \times 10^3$	$1.02 \times 10^5$	$3.46 \times 10^4$	7.24	2.56
GB-04	Modern	$1.61 \times 10^4$	$1.39 \times 10^3$	Below Detection Limit		----	----
MC-03	Modern	$1.98 \times 10^4$	$1.66 \times 10^3$	$1.20 \times 10^5$	$1.19 \times 10^4$	6.06	0.79
SS-02	Modern	$2.79 \times 10^4$	$2.01 \times 10^3$	$1.73 \times 10^5$	$1.25 \times 10^4$	6.19	0.63
SS-03	Modern	$2.63 \times 10^4$	$1.78 \times 10^3$	$1.72 \times 10^5$	$1.31 \times 10^4$	6.55	0.67
SS-04	Modern	$4.76 \times 10^4$	$2.16 \times 10^3$	$2.68 \times 10^5$	$3.51 \times 10^4$	5.64	0.78
GB-06	Bedrock	$7.33 \times 10^4$	$3.90 \times 10^3$	$5.91 \times 10^5$	$2.90 \times 10^4$	8.05	0.58

LBD19-46 (0 cm)	Bedrock	$5.02 \times 10^4$	$1.87 \times 10^3$	$3.30 \times 10^5$	$1.37 \times 10^4$	6.57	0.37
LBD19-47 (10 cm)	Bedrock	$3.89 \times 10^4$	$1.76 \times 10^3$	$2.49 \times 10^5$	$1.32 \times 10^4$	6.41	0.43
LBD19-48 (20 cm)	Bedrock	$4.36 \times 10^4$	$2.89 \times 10^3$	$2.51 \times 10^5$	$1.86 \times 10^4$	5.77	0.55
LBD19-49 (50 cm)	Bedrock	$2.48 \times 10^4$	$1.83 \times 10^3$	$1.57 \times 10^5$	$9.49 \times 10^3$	6.34	0.58
LBD19-50 (100 cm)	Bedrock	$1.31 \times 10^4$	$1.16 \times 10^3$	$8.24 \times 10^4$	$5.25 \times 10^3$	6.27	0.63
LBD19-51 (150 cm)	Bedrock	$7.24 \times 10^3$	$7.07 \times 10^2$	$5.68 \times 10^4$	$5.09 \times 10^3$	7.85	0.92
LBD19-52 (190 cm)	Bedrock	$5.94 \times 10^3$	$6.07 \times 10^2$	$3.51 \times 10^4$	$4.35 \times 10^3$	5.90	0.85

Nuclide concentrations and uncertainties incorporate blank corrections. Uncertainties are  $1\sigma$ .

Depths of samples LBD19-46 to LBD19-52 in bedrock depth profile are given after sample name.

The bedrock sample (GB-06) had the highest concentration of  $^{10}\text{Be}$  ( $7.33 \pm 0.39 \times 10^4$  atoms  $\text{g}^{-1}$ ) and  $^{26}\text{Al}$  ( $5.91 \pm 0.29 \times 10^5$  atoms  $\text{g}^{-1}$ ) that we measured. The coastal bedrock depth profile had a surface concentration of  $5.02 \pm 0.19 \times 10^4$   $^{10}\text{Be}$  atoms  $\text{g}^{-1}$  and  $3.30 \pm 0.14 \times 10^5$   $^{26}\text{Al}$  atoms  $\text{g}^{-1}$  (Figure 4). Concentrations of both nuclides decrease exponentially with depth in the bedrock profile, with e-folding lengths of approximately 175 to 190  $\text{g cm}^{-2}$ , longer than would be expected from spallation production alone (165  $\text{g cm}^{-2}$ ). We note that the sample at depth 10 cm does not fit well on the profile. It was taken to the left side of the profile (Figure 2E) and may have had a different cover history.

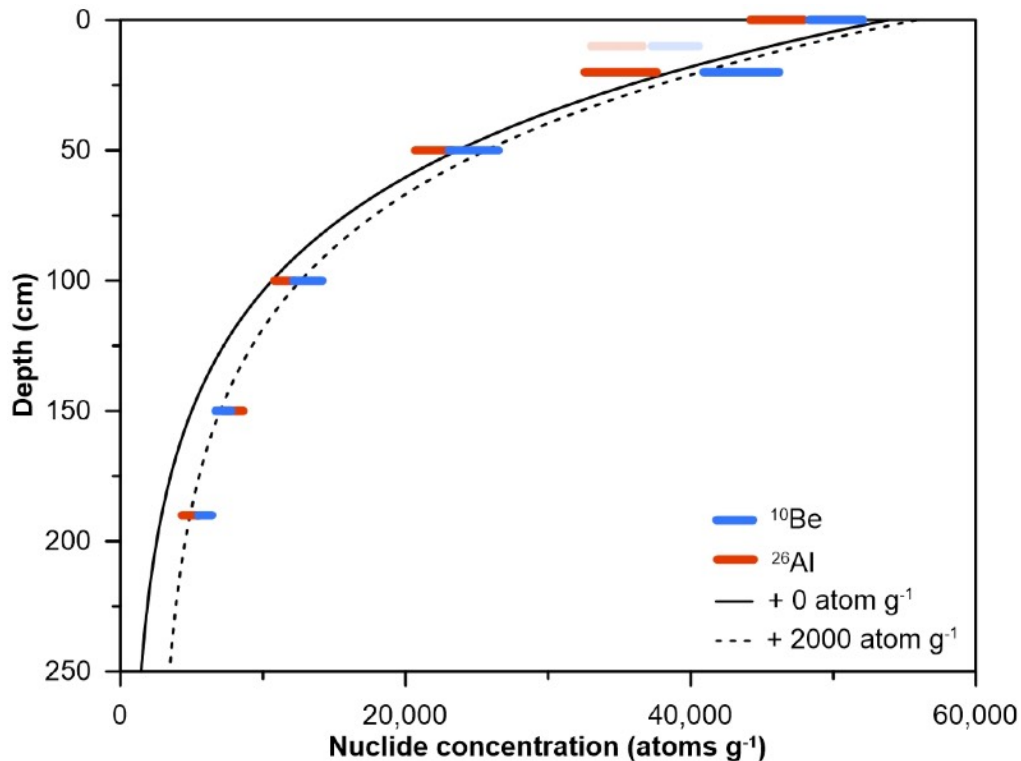


**Figure 4.** Depth profile in bedrock with modelled fit for 11.5 kyr of surface exposure and inheritance of 0 and 2000 atoms  $\text{g}^{-1}$ . Symbols extend to 1 standard deviation analytic uncertainty. Solid line is fit with no inherited nuclides. Dashed line assumes uniform 2000 atoms  $\text{g}^{-1}$  inheritance for  $^{10}\text{Be}$ .  $^{26}\text{Al}$  was scaled to equivalent  $^{10}\text{Be}$  concentration assuming  $^{26}\text{Al}/^{10}\text{Be}$  ratio of 7.3. Shaded sample collected away from profile (Figure 2E) and not considered in fit.

### 5.1. $^{10}\text{Be}$ and $^{26}\text{Al}$ Concentrations in Deglacial Samples Corrected for Holocene Exposure

After correcting for Holocene exposure, there is significant difference between the concentration of  $^{10}\text{Be}$  in deglacial (mean, 1SD,  $n=10$ ;  $1.87 \pm 1.41 \times 10^4$  atoms  $\text{g}^{-1}$ ) and modern ( $n=11$ ,  $3.31 \pm 1.57 \times 10^4$  atoms  $\text{g}^{-1}$ ) sediment samples ( $p = 0.02$ ) (Table 4, Figure 5). For  $^{26}\text{Al}$ , the concentration of deglacial ( $1.20 \pm 1.04 \times 10^5$  atoms  $\text{g}^{-1}$ ) and modern ( $2.12 \pm 1.18 \times 10^5$  atoms  $\text{g}^{-1}$ ) samples are also significantly different ( $p = 0.04$ ) (Figure 4B). The modern samples are more variable in  $^{10}\text{Be}$  concentration, with an interquartile range (IQR) of  $2.80 \times 10^4$  atoms  $\text{g}^{-1}$  compared to the IQR of  $8.17 \times 10^3$  atoms  $\text{g}^{-1}$  for Holocene exposure-corrected deglacial samples.

Both the bedrock sample (GB-06) and the bedrock depth profile contain nuclides inherited from prior exposure. Inferring an exposure age of 8.1 ky from maps of Dalton et al. (2020), and correcting for Holocene exposure with no erosion (the outcrop is smooth and rounded, Figure 2C), GB-06 contains  $1.83 \times 10^4$  atoms  $\text{g}^{-1}$  of inherited  $^{10}\text{Be}$  and  $2.17 \times 10^5$  atoms  $\text{g}^{-1}$  of inherited  $^{26}\text{Al}$ . Nuclide profiles modelled to reflect Holocene exposure for best fit the profile data when they include  $\sim 2 \times 10^3$  atoms  $\text{g}^{-1}$  of inherited  $^{10}\text{Be}$  and  $\sim 1.4 \times 10^4$  atoms  $\text{g}^{-1}$  of inherited  $^{26}\text{Al}$  (Figure 4).

Our analysis of previously published  $^{10}\text{Be}$  data suggests that inheritance of cosmogenic nuclides from prior period(s) of exposure is common in Quebec and Labrador. Over half of bedrock samples ( $n = 26$  of 46, including our new sample GB-06) and a third of boulder samples ( $n = 65$  of 192) contain significant concentrations of inherited nuclides, which we consider  $>3 \times 10^3$  atoms  $\text{g}^{-1}$  because that is the median analytical uncertainty in the dataset. The

mean and range of inherited nuclide concentrations are larger for samples of bedrock (mean =  $1.21 \times 10^5$  atoms  $g^{-1}$ ; IQR =  $8.04 \times 10^4$  atoms  $g^{-1}$ ) than boulders (mean =  $1.40 \times 10^4$  atoms  $g^{-1}$ ; IQR =  $1.28 \times 10^4$  atoms  $g^{-1}$ ).

## 5.2. $^{26}Al/^{10}Be$ Ratios

The error-weighted mean of  $^{26}Al/^{10}Be$  ratios for deglacial sand (correcting for Holocene nuclide production) and modern sediment samples ( $6.1 \pm 1.2$  and  $6.6 \pm 0.5$ , respectively, one standard deviation) are lower than the measured Arctic production ratio of  $7.3 \pm 0.3$  (Figure 5C,  $p = 0.01$ , Corbett et al., 2017). The  $^{26}Al/^{10}Be$  ratios for deglacial samples are more variable (IQR = 2.41) than ratios measured in modern stream samples (IQR = 0.78, Figure 5C).

The  $^{26}Al/^{10}Be$  of deglacial samples exhibit a significant, positive linear trend with increasing distance from the center of the QLID ( $r^2 = 0.45$ ,  $p = 0.03$ ) (Figure 5). The five samples closest to the center of the ice dome ( $5.2 \pm 0.8$ ) have lower error-weighted average  $^{26}Al/^{10}Be$  ratios than five samples farther away ( $7.0 \pm 0.7$ , Figure 6). Modern samples, in contrast, exhibit no spatial trend in  $^{26}Al/^{10}Be$  ratios. Tukey HSD tests show a significant difference between  $^{26}Al/^{10}Be$  ratios in deglacial samples closest to and further from the center of the ice dome (both tests:  $p < 0.01$ ).

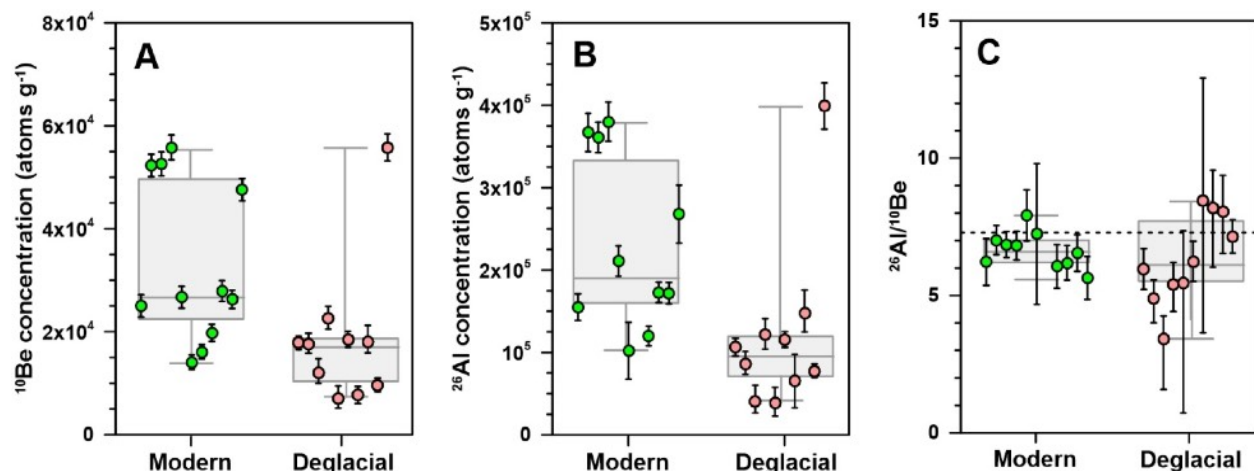


**Figure 5.** Comparison of modern and Holocene-exposure-corrected deglacial samples. (A)  $^{10}Be$  concentrations, (B)  $^{26}Al$  concentrations, and (C)  $^{26}Al/^{10}Be$  ratios for deglacial (Holocene-corrected) and modern samples. The dashed line in panel C indicates the empirical production ratio (7.3) at high latitudes from Corbett et al. (2017). Points represent individual samples with  $1\sigma$  propagated errors for modern (green) and deglacial (pink) samples. Box and whisker plots are shown for each dataset with whiskers going to the smallest and highest values. The box extends from the 25<sup>th</sup> to the 75<sup>th</sup> percentiles. The line in the middle of each box is the median.

**Table 4. Holocene Exposure-Corrected Isotopic Data for Deglacial Samples**

Sample Name	Distance from Laboratory City	Inherited $^{10}\text{Be}$ (atoms $\text{g}^{-1}$ )	$^{10}\text{Be}$ Uncertainty (atoms $\text{g}^{-1}$ ) <sup>a</sup>	Inherited $^{26}\text{Al}$ (atoms $\text{g}^{-1}$ )	$^{26}\text{Al}$ Uncertainty (atoms $\text{g}^{-1}$ ) <sup>a</sup>	Inherent $^{26}\text{Al}/^{10}\text{Be}$	$^{26}\text{Al}/^{10}\text{Be}$ Uncertainty <sup>a</sup>
L C-02	109	$1.76 \times 10^4$	$(-2.15, +1.74) \times 10^3$	$8.61 \times 10^4$	$(-1.51, +1.25) \times 10^4$	4.90	-0.89, +0.67
L C-04	162	$1.20 \times 10^4$	$(-2.77, +1.98) \times 10^3$	$4.09 \times 10^4$	$(-1.93, +1.42) \times 10^4$	3.41	-1.84, +0.84
L C-05	188	$2.26 \times 10^4$	$(-2.35, +2.07) \times 10^3$	$1.22 \times 10^5$	$(-1.92, +1.77) \times 10^4$	5.40	-0.98, +0.81
C F-02	221	$1.78 \times 10^4$	$(-1.31, +1.30) \times 10^3$	$1.07 \times 10^5$	$(-1.08, +1.08) \times 10^4$	5.97	-0.75, +0.74
M C-01	309	$7.06 \times 10^3$	$(-2.46, +1.88) \times 10^3$	$3.85 \times 10^4$	$(-1.90, +1.57) \times 10^4$	5.45	-4.73, +1.90
GB-05	361	$1.81 \times 10^4$	$(-3.15, +2.19) \times 10^3$	$1.48 \times 10^5$	$(-2.78, +2.31) \times 10^4$	8.19	-2.16, +1.38
GB-03	403	$7.73 \times 10^3$	$(-1.69, +1.68) \times 10^3$	$6.54 \times 10^4$	$(-3.23, +3.23) \times 10^4$	8.46	-4.81, +4.47

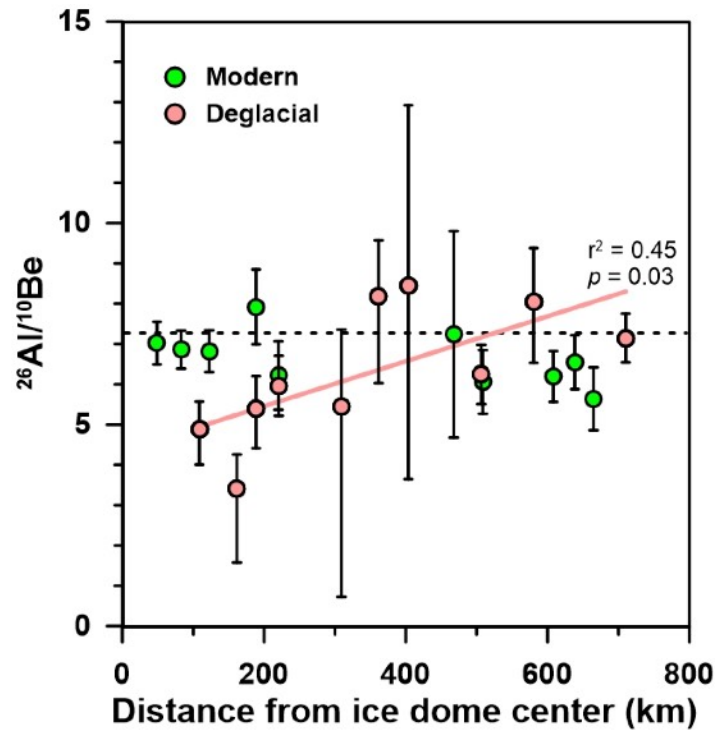
M C- 02	506		1.85 x 10 <sup>4</sup>	(-1.54, +1.54) x 10 <sup>3</sup>	1.16 x 10 <sup>5</sup>	(-9. 56, +9. 56) x 10 <sup>2</sup>	6. 24	-0. 73 , +0 .7
S S- 01		580	9.6 5 x 10 <sup>3</sup>	(-1. 37, +1.2 9) x 10 <sup>3</sup>	7.76 x 10 <sup>4</sup>	(-8. 65, +8. 00) x 10 <sup>2</sup>	8. 04	-1. 51 , +1 .3
S S- 05		710		(-2.63, +2.63) x 10 <sup>3</sup>	3. 99 x 10 <sup>5</sup>	(-2. 81, +2.8 1) x 10 <sup>4</sup>	7. 15	-0. 61 , +0 .6
GB- 06	285	1.07 x 10 <sup>4</sup>	3.90 x 10 <sup>3</sup>	1.65 x 10 <sup>5</sup>		2.90 x 10 <sup>4</sup>	15.4	6.24

<sup>a</sup>Uncertainties account for both analytical and sample depth uncertainties

. The depth uncertainties

in combination with nonlinear production rate changes with depth yield asymmetrical nuclide uncertainties. Uncertainties are  $1\sigma$ .

Figure 6.



$^{26}\text{Al}/^{10}\text{Be}$  ratios versus distance from center of the QLID at Labrador City. Deglacial data are corrected for Holocene nuclide production and fit with a trendline. Error bars are  $1\sigma$ . Dashed line shows production ratio at high latitudes (7.3, Corbett et al., 2017).

## 6. Discussion

Measurements of in situ-produced  $^{10}\text{Be}$  and  $^{26}\text{Al}$ , presented here and in previously published papers, indicate that many samples of bedrock (57%), erratic boulders (34%), and deglacial sediment (100%) collected from terrain once covered by the QLID of the LIS contain cosmogenic nuclides accumulated during periods of exposure prior to the last deglaciation. This finding differs from that of Heyman et al. (2011) who 15 years prior to our work, suggested that “few boulders from the paleo-ice sheets have exposure ages significantly older than independently known deglaciation ages, indicating that prior exposure is of limited significance.” Their compilation was geographically broader, suggesting that the QLID may differ for other glaciated terrains. Or our finding may reflect numerous additional measurements have been made since the publication of Heyman et al. (2011), a time over which cosmogenic nuclide measurement precision has greatly improved and the number of pertinent other dates has increased. As Heyman et al. (2011) point out, such inheritance, if not detected and corrected for, has the potential to bias cosmogenic exposure ages high, including those from exposed rock and glacial deposits.

### 6.1 Differences in nuclide inheritance between sample types

Compilation of extant cosmogenic data shows that samples collected from erratic boulders contain lower average concentrations of inherited nuclides (14,000 atoms  $\text{g}^{-1}$ ) than those collected from bedrock outcrops (120,700 atoms  $\text{g}^{-1}$ ) and deglacial sediment (18,800 atoms  $\text{g}^{-1}$ , Figure 7). Of the 192 reported boulder analyses, we calculate that 65 boulder samples (34% of total) contain  $^{10}\text{Be}$  inherited from pre-LGM periods of exposure on the basis of having  $>3000$  atoms  $\text{g}^{-1}$  of  $^{10}\text{Be}$  (the median analytical uncertainty) above that produced during deglacial exposure as determined from Dalton et al.'s (2020) isochrons. The average boulder inheritance is equal to  $\sim 1800$  years of surface exposure, a value skewed high by relatively few boulders with large concentrations of inherited nuclides. In contrast, the median inheritance for sampled boulders is negative,  $-4000$  atoms  $\text{g}^{-1}$ , resulting in a median boulder age about 650 years younger than Dalton et al.'s (2020) radiocarbon based chronology. Such a discrepancy between boulder exposure ages and radiocarbon ages of organic material could reflect boulder surface erosion, boulder burial by snow or till (Schildgen et al., 2005),  $^{10}\text{Be}$  production rate uncertainty (Balco et al., 2009), or incorporation of old carbon in radiocarbon dated samples (see references in Halsted et al., 2024).

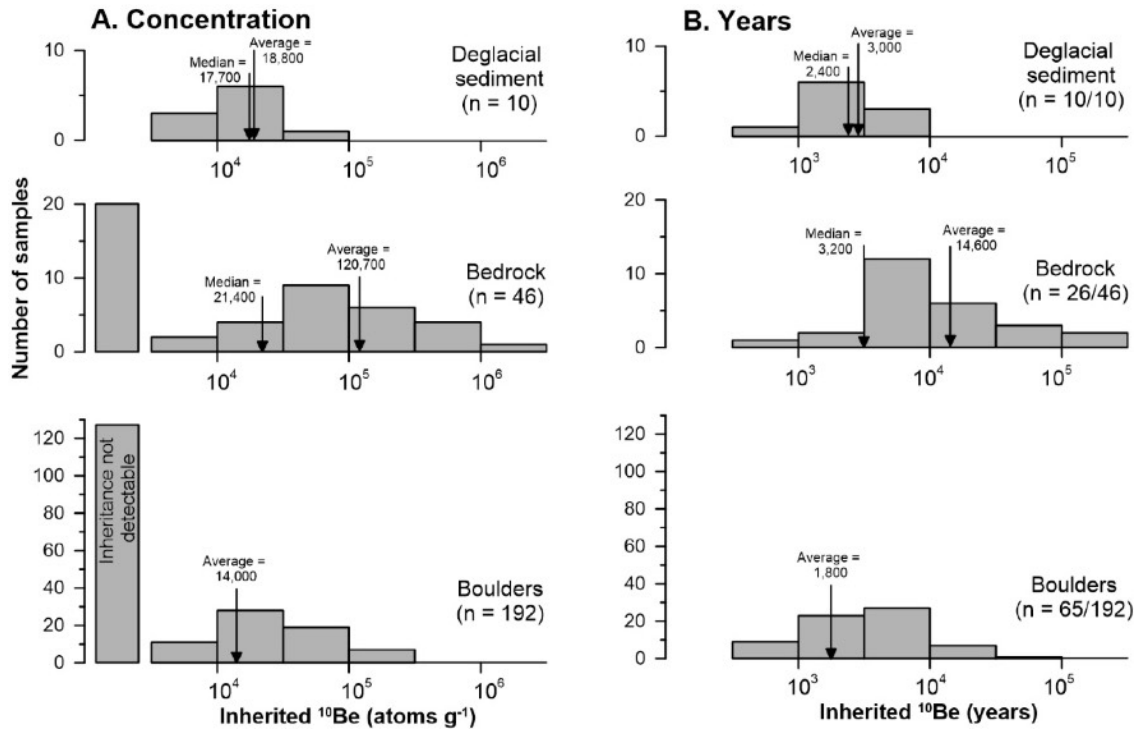


**Figure 7.** Histograms (logarithmic) of inherited  $^{10}\text{Be}$  in deglacial sediment (this study), glaciated bedrock (this study and others), and erratic boulders (other studies) sampled from eastern Canadian landscapes once covered by the QLID of the LIS. A. Inheritance (atoms  $\text{g}^{-1}$ ). B. Inheritance expressed as years of surface exposure calculated using site-specific  $^{10}\text{Be}$  production rates to remove elevation dependence of nuclide production rates. Sample count, average, and median values indicated with arrows. Values  $< 3000$  atoms  $\text{g}^{-1}$ , the median uncertainty in measurements, are considered to have no detectable inheritance and are counted as zero for statistical analysis.

We find that 26 of 46 sampled bedrock outcrops (57%) contain detectable  $^{10}\text{Be}$  (mean = 120,700 atoms  $\text{g}^{-1}$ ; median = 21,400 atoms  $\text{g}^{-1}$ ) inherited from pre-LGM periods of exposure. Considered as exposure time, this is an average inheritance for bedrock samples of 14,600 years. Because the distribution is skewed, the median inheritance, when considered as a surface exposure time, is less—3200 years (Figure 7). Lower mean and median concentrations of inherited nuclides in erratic boulders than in exposed bedrock from beneath the former QLID suggest that the boulders were quarried from below the present-day bedrock surface, are preferentially derived from more erosive areas of the ice sheet, and/or were reworked from deposits deep enough that interglacial exposure to cosmic radiation was insufficient to create high concentrations of  $^{10}\text{Be}$ .

All 10 deglacial sand samples (100%) contain inherited nuclides (median = 17,700 atoms  $\text{g}^{-1}$ ; mean = 18,800 atoms  $\text{g}^{-1}$ ), the equivalent of 2400 and 3000 years of surface exposure (Figure 7). Unlike the distribution of boulder and bedrock sample  $^{10}\text{Be}$  concentrations, those of deglacial sand samples are not skewed as indicated by the similarity of the mean and median. This similarity likely reflects the physical mixing of thousands of sand grains included in the sediment samples, each with its own idiosyncratic burial and exposure history.

A sensitivity analyses shows that our finding of nuclide inheritance is robust to uncertainty in the time/retreat distance model that we used to correct for post-depositional nuclide production. For surface boulder and

bedrock samples, if Dalton et al.'s retreat chronology were 10% too old, then the number of such samples with inheritance above analytical uncertainty ( $3,000 \text{ atoms g}^{-1}$ ) would increase from 90 to 120. Conversely, if the Dalton et al., (2020) model reported deglacial ages that were 10% too young, then the number of samples with inheritance would decrease from 90 to 75. For buried deglacial sand samples, the influence of the age model is less than for boulders and bedrock collected at the surface because the cosmic-flux is strongly attenuated with depth.

Because isostatic uplift in response to deglaciation has raised sample sites to higher elevations than they were at the time of deglaciation, nuclide production rates have changed over time (Jones et al., 2019). Using the data provided in Dalton et al. (2023), we calculated that accounting for such post glacial uplift would increase the concentration of nuclides inherited at initial exposure by  $3400 \pm 2400 \text{ atoms g}^{-1}$ . While such a correction is uncertain, it suggests that our estimates of nuclides inherited from periods of prior exposure are likely conservative.

## **6.2 Spatial variability in ice sheet erosion depth**

Our compilation of data from 248 samples analyzed for cosmogenic nuclides indicates that the QLID of the LIS did not deeply or uniformly erode its bed, nor did it effectively remove nuclides produced in sediment and rock exposed during prior interglacial periods (Figure 8). The broad distribution of inherited  $^{10}\text{Be}$  concentrations in bedrock is consistent with spatially variable ice sheet erosivity and/or varying thickness of interglacial sediment cover shielding the underlying rock from cosmic rays when the ice was gone and has been noted by others, particularly at high elevations in the eastern part of the study area (Marquette et al., 2004; Staiger et al., 2005).

Subglacial process modeling over eastern North America (Melanson et al., 2013) suggests a variably erosive LIS in Quebec and Labrador during the last glacial cycle consistent with our findings. Melanson et al., (2013) suggest that total erosion per glacial cycle, predicted using empirical abrasion and quarrying laws, ranges from near zero under the center of the Quebec-Labrador dome to  $\geq 10 \text{ m}$  along parts of its Atlantic and St. Lawrence margin. Melanson et al.'s numerical modeling of the Quebec-Labrador region exhibits similar minima for both basal sliding speed and total ice movement integrated over the last glacial cycle – both variables related to the efficacy of glacial erosion. Simulated ice sliding distances (the integrated basal velocity over the last glacial cycle in millions of meters, Mm) are near zero in the center of our study area, 1 Mm near Goose Bay, and 3 Mm along the St. Lawrence estuary – an order of magnitude less than for the Hudson Strait ice stream and southern LIS lobes (Melanson et al., 2013).

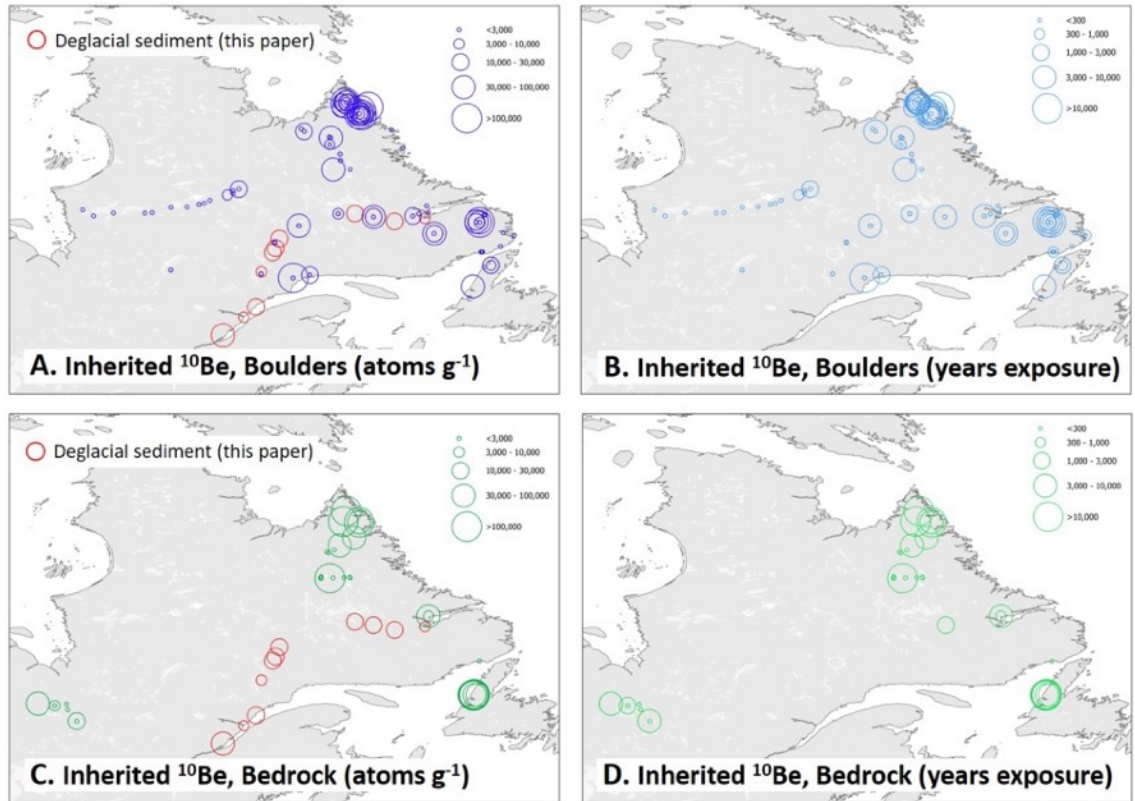


**Figure 8.** Spatial distribution of inheritance interpreted from published data corrected using deglacial age model of Dalton et al. (2020). A. Boulder data, atoms  $g^{-1}$  inherited  $^{10}Be$ . B. Boulder data, inherited years equivalent surface exposure. C. Bedrock data, atoms  $g^{-1}$  inherited  $^{10}Be$ . B. Bedrock data, inherited years equivalent surface exposure. Red circles are deglacial sediment data (this paper). Inheritance keyed to circle diameter.

The average concentration of inherited nuclides we measured in LIS deglacial sediment (18,800  $^{10}Be$  atoms  $g^{-1}$ ) is several times higher than the average measured in sediment shed by the Greenland Ice Sheet today ( $\sim 6,500$   $^{10}Be$  atoms  $g^{-1}$ , Nelson et al., 2014) but much lower than those deposited by the LIS in the midwestern United States ( $\sim 60,000$   $^{10}Be$  atoms  $g^{-1}$ , Balco, 2005). The low concentrations of  $^{10}Be$  in sediment issuing from the Greenland Ice Sheet (as well as low  $^{26}Al/^{10}Be$  ratios  $\sim 4.5$ , Bierman et al., 2016) reflect continuous ice cover through many Pleistocene interglacials and erosive warm-based ice in areas from which sediment is sourced. In contrast, the high concentrations of  $^{10}Be$  in deglacial sediment originating from the southern margin of the Keewatin Ice Dome in Minnesota (Balco, 2005) suggest that ice there was frequently absent and when present, only weakly erosive. Some data suggest that in central North America the LIS was at least in part, cold-based near the margin (c.f., Colgan et al., 2002).

### 6.3 Implications for sample collection and surface exposure dating

The new and compiled data have implications for sample collection and interpretation in areas once covered by now-vanished ice sheets, specifically the QLID of the LIS. The compiled data show clearly that sampling boulders rather than bedrock is most likely to minimize the influence on calculated landform age of

nuclides inherited from exposure prior to the last deglaciation. Because the distributions of inherited  $^{10}\text{Be}$  concentrations in both the bedrock and boulder populations are skewed (Figure 7), extreme outliers are easily detectable. Indeed, Ullman et al. (2016) excluded 10 of 65 boulder samples because of their unusually high concentration of  $^{10}\text{Be}$ . Couette et al., (2023) similarly excluded 5 of 37 samples in eastern Labrador because of high  $^{10}\text{Be}$  concentrations.

However, small concentrations of inherited nuclides, likely the result of deeply penetrating muons, are more difficult to detect and thus correct for. Such inheritance could skew slightly the average age of an exposure age data set. In that regard, the depth profile data (samples LBD19-46-52) are illustrative because they are consistent with several thousand atoms  $\text{g}^{-1}$  of inherited nuclides at depth of several meters (Figure 4). Such inheritance would increase exposure ages of plucked boulders and glacially eroded outcrops by hundreds of years (a phenomenon noted by Ullman et al. (2016) who reported that  $^{10}\text{Be}$ -based deglacial chronology was older than radiocarbon-based estimates of local deglaciation by centuries, their Figure 7). While radiocarbon age lags are attributed to delayed colonization of the landscape by vegetation following deglaciation (e.g., Peteet et al., 2012), the nuclide inheritance we find in Quebec and Labrador suggests that in this region, some  $^{10}\text{Be}$  ages will be too old. The overall agreement of the Ullman et al. (2016) cosmogenic ages with those of Dalton et al. (2022) and Dyke (2004) suggest that after removal of obvious outliers, a population of boulder dates, screened for outliers, is likely to be robust in our study area at ky resolution.

#### **6.4 Interglacial presence of QLID of the LIS and $^{26}\text{Al}/^{10}\text{Be}$ ratio of IRD**

Finding  $^{26}\text{Al}/^{10}\text{Be}$  ratios below the nominal arctic surface production ratio of 7.3 (Corbett et al., 2017) in quartz IRD from North Atlantic Heinrich layers, LeBlanc et al. (2023) suggested that ice sheet remnants may have lingered in parts of eastern Canada for the majority of Pleistocene interglacials. While Heinrich layer sediment was predominantly delivered to the ocean by the Hudson Strait ice stream, the quartz IRD that LeBlanc et al. (2023) analyzed most likely came from interior areas of the LIS (where crystalline rocks crop out) as opposed to Hudson Strait, which is primarily underlain by carbonate rocks (Bond et al., 1992).

Depressed  $^{26}\text{Al}/^{10}\text{Be}$  ratios in the Holocene exposure-corrected deglacial sediment that we sampled suggest ice lingered near the Labrador City (the center of the ice dome) for at least some interglacial periods, shielding rock and sediment below from cosmic rays (Figure 6). In contrast, the higher  $^{26}\text{Al}/^{10}\text{Be}$  ratios in deglacial sediment further from the center of the ice dome are consistent with repeated exposure during interglacials. Thus, the quartz analyzed by LeBlanc et al. (2023) is unlikely to have been sourced from much of the area we sampled in southeastern Canada.

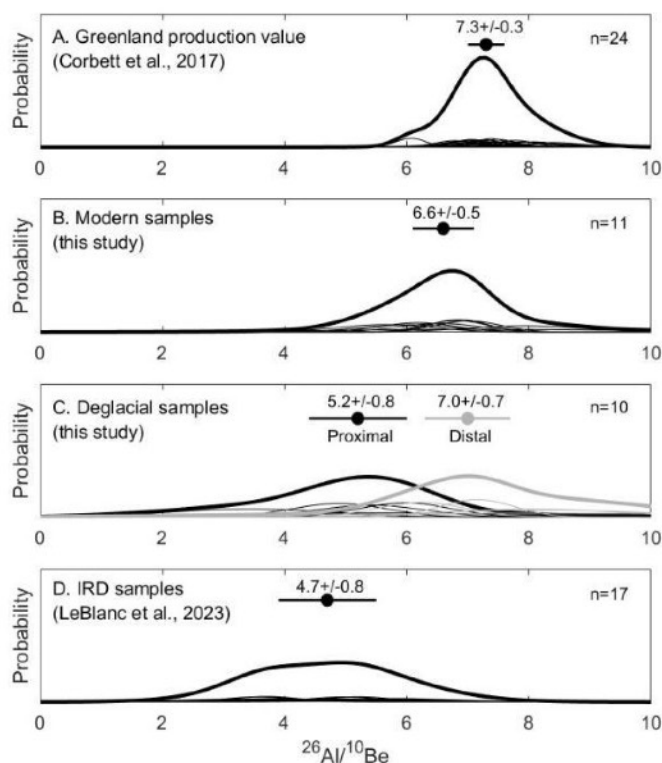


**Figure 9. Summed probability plots of  $^{26}\text{Al}/^{10}\text{Be}$  ratios for Arctic samples.** A. Samples with simple exposure histories in Greenland (Corbett et al., 2017). B. Modern stream sediment (this study). C. Deglacial samples corrected for Holocene exposure; black 5 samples most proximal to Labrador City (center of the dome); gray 5 samples are most distal (this study). D. IRD samples from North Atlantic (LeBlanc et al., 2023). Analytical error-weighted mean and 1 SD uncertainty above each plot.

It is possible that incorporation of IRD occurred primarily toward the center of the QLID and not closer to the margins. It is also possible that the IRD sampled by LeBlanc et al. (2023) was sourced from a wider area (the Keewatin Dome and/or Baffin Island) where samples of sediment (Balco, 2005) and those taken from outcrops (Marsella et al., 2000) have sufficiently low  $^{26}\text{Al}/^{10}\text{Be}$  ratios to match those measured by LeBlanc et al. (2023). Low ratios would also result if IRD were stored in Hudson Bay for  $\sim 1$  Ma before transport to the deep sea, during which time  $^{26}\text{Al}$  and  $^{10}\text{Be}$  would decay and the  $^{26}\text{Al}/^{10}\text{Be}$  ratio lower. More extensive sampling of eastern Canada, including Quebec-Labrador, and further north near Hudson Bay and Baffin Island, would provide further evidence on how persistent different sectors of the eastern LIS were during Pleistocene interglacials.

### 6.5 Sediment Sourcing in Modern Rivers

We estimate the percentage of sediment derived from erosion of deglacial materials using a two-component, linear-mixing model based on the measured average concentrations of  $^{10}\text{Be}$  in both river and deglacial sediment and assumptions about nuclide production since deglaciation. One component is deglacial deposits which, based on our sampling, contain an average of  $22.5 \times 10^3$   $^{10}\text{Be}$  atoms  $\text{g}^{-1}$  and enter rivers by bank incision (Figure

2A). The second component is surficial materials which, when eroded, enter the drainage network. Since we did not sample these surficial materials directly, we calculate their  $^{10}\text{Be}$  concentration by assuming that, at the time of deglaciation (the beginning of exposure), surface sediment contained the average Holocene exposure-corrected concentration of  $^{10}\text{Be}$  for deglacial sediment ( $18.7 \times 10^3$   $^{10}\text{Be}$  atoms  $\text{g}^{-1}$ ). We then use the average deglacial age of 9.32 ka for our field area and the average  $^{10}\text{Be}$  surface production rate ( $7.82$  atoms  $\text{y}^{-1}$   $\text{g}^{-1}$ ) to calculate that surface material gained about  $7.3 \times 10^4$   $^{10}\text{Be}$  atoms  $\text{g}^{-1}$  since deglaciation. The surface-exposed end member therefore contains  $91.6 \times 10^3$   $^{10}\text{Be}$  atoms  $\text{g}^{-1}$ .

Knowing that modern sediment contains on average  $33.1 \times 10^3$   $^{10}\text{Be}$  atoms  $\text{g}^{-1}$ , the two-component mixing model suggests that about 85% of sediment in eastern Quebec and Labrador rivers today is derived from incision of glacial deposits and the remaining about 15% comes from erosion of surficial sediment and bedrock. Our findings for eastern Quebec and Labrador are similar to those of Balco (2005) in Minnesota. In that previously glaciated region, they suggest most sediment carried by contemporary rivers comes from incision of glacial deposits. Our finding is also consistent with the low sediment yield of forested upland terrains in other glaciated areas of the LIS (e.g., Dethier et al., 2018).

## 7.0 Conclusions

Analysis of cosmogenic  $^{10}\text{Be}$  and  $^{26}\text{Al}$  in deglacial ( $n=10$ ) and modern ( $n=11$ ) sediment samples, in a bedrock depth profile ( $n=7$ ), in previously-studied boulders and bedrock samples ( $n=237$ ), and in one bedrock sample we collected, indicates that nuclides produced during prior interglacial exposures are commonplace in samples from beneath the now-vanished QLID of the LIS. These isotopic data indicate erosion depths in bedrock likely average at most a few meters per glacial cycle and that regolith generated and exposed during previous glacial and interglacial cycles was not completely removed from the terrestrial landscape during the last glaciation. Such inheritance explains outliers in previously published data sets. Comparison of data sets in which such outliers were removed shows that average ages match well those suggested by radiocarbon dating. Boulders in the area covered by the QLID appear to carry, on average, lower concentrations of inherited nuclides than bedrock outcrops suggesting that dating studies with limited resources may benefit from dating boulders rather than bedrock. On average, nuclide concentrations in modern fluvial sediment are only slightly higher than those in deglacial sediment, implying most sand, transported by rivers today in landscapes once covered by the QLID, is sourced from eroding banks composed of glacial deposits rather than surrounding land surfaces.

## Author contribution

Bierman and Shakun conceived and designed the study. Cavnar, LeBlanc, and Shakun collected samples. Cavnar performed sample preparation under the supervision of Corbett. Caffee assisted with statistical analysis and oversaw measurement of cosmogenic nuclides via AMS at PRIME Lab. Couette and Ghienne collected the bedrock depth profile samples. Couette performed sample preparation and data analysis under the supervision of Van der Woerd. Cavnar drafted the initial manuscript and performed initial data reduction and statistical analysis. Shakun and Bierman performed data compilation and inheritance analysis. All authors assisted with conceptual design of figures, manuscript organization, and editing. Bierman, Shakun, and LeBlanc revised the manuscript after initial peer review.

## Competing Interests

The authors declare that they have no conflict of interest.

## Acknowledgements

We thank the 2022 field sampling team including Juliana Souza, Halley Mastro, and Cat Collins. Funding for this research was provided by NSF-EAR-2300560, 2116209, 2114629, and 1735676 awards to Bierman and Corbett, 2116208 to Shakun, NSF-OPP-PRF 2420274 post-doctoral fellowship to LeBlanc, NSERC grants to Lajeunesse, and institutional grants to Ghienne. The French national AMS facility ASTER (CEREGE) is supported by the INSU/CNRS, the French MESR, and the CEA institute. We thank G. Aumaître and K. Keddadouche for the AMS measurements at ASTER.

## References Cited

- Alley, R. B., Cuffey, K. M., and Zoet, L. K.: Glacial erosion: status and outlook, *Annals of Glaciology*, 60, 1–13, <https://doi.org/10.1017/aog.2019.38>, 2019.
- Amani, M., Mahdavi, S., Afshar, M., Brisco, B., Huang, W., Mohammad Javad Mirzadeh, S., White, L., Banks, S., Montgomery, J., and Hopkinson, C.: Canadian wetland inventory using Google Earth Engine: the first map and preliminary results, *Remote Sensing*, 11, 842, <https://doi.org/10.3390/rs11070842>, 2019.
- Andrews, J. T. and Tyler, K.: The observed postglacial recovery of Québec and Nouveau-Québec Since 12,000 BP, *Géographie physique et Quaternaire*, 31, 389–400, <https://doi.org/10.7202/1000286ar>, 2011.
- Balco, G.: Dating Plio-Pleistocene glacial sediments using the cosmic-ray-produced radionuclides  $^{10}\text{Be}$  and  $^{26}\text{Al}$ , *American Journal of Science*, 305, 1–41, <https://doi.org/10.2475/ajs.305.1.1>, 2005.
- Balco, G. and Rovey, C. W.: An isochron method for cosmogenic-nuclide dating of buried soils and sediments, *American Journal of Science*, 308, 1083–1114, <https://doi.org/10.2475/10.2008.02>, 2008.
- Balco, G. and Rovey, C. W.: Absolute chronology for major Pleistocene advances of the Laurentide Ice Sheet, *Geology*, 38, 795–798, <https://doi.org/10.1130/G30946.1>, 2010.
- Balco, G., Stone, J. O. H., Porter, S. C., and Caffee, M. W.: Cosmogenic-nuclide ages for New England coastal moraines, Martha's Vineyard and Cape Cod, Massachusetts, USA, *Quaternary Science Reviews*, 21, 2127–2135, [https://doi.org/10.1016/S0277-3791\(02\)00085-9](https://doi.org/10.1016/S0277-3791(02)00085-9), 2002.
- Balco, G., Stone, J. O., Lifton, N. A., and Dunai, T. J.: A complete and easily accessible means of calculating surface exposure ages or erosion rates from  $^{10}\text{Be}$  and  $^{26}\text{Al}$  measurements, *Quaternary Geochronology*, 3, 174–195, <https://doi.org/10.1016/j.quageo.2007.12.001>, 2008.
- Balco, G., Briner, J., Finkel, R. C., Rayburn, J. A., Ridge, J. C., and Schaefer, J. M.: Regional beryllium-10 production rate calibration for late-glacial northeastern North America, *Quaternary Geochronology*, 4, 93–107, <https://doi.org/10.1016/j.quageo.2008.09.001>, 2009.
- Balter-Kennedy, A., Schaefer, J. M., Balco, G., Kelly, M. A., Kaplan, M. R., Schwartz, R., Oakley, B., Young, N. E., Hanley, J., and Varuolo-Clarke, A. M.: The Laurentide Ice Sheet in southern New England and New York during and at the end of the Last Glacial Maximum: a cosmogenic-nuclide chronology, *Clim. Past*, 20, 2167–2190, <https://doi.org/10.5194/cp-20-2167-2024>, 2024.

- Barth, A. M., Marcott, S. A., Licciardi, J. M., and Shakun, J. D.: Deglacial Thinning of the Laurentide Ice Sheet in the Adirondack Mountains, New York, USA, Revealed by<sup>36</sup>Cl Exposure Dating, *Paleoceanog and Paleoclimatol*, 34, 946–953, <https://doi.org/10.1029/2018PA003477>, 2019.
- Batchelor, C. L., Margold, M., Krapp, M., Murton, D. K., Dalton, A. S., Gibbard, P. L., Stokes, C. R., Murton, J. B., and Manica, A.: The configuration of Northern Hemisphere ice sheets through the Quaternary, *Nat Commun*, 10, 3713, <https://doi.org/10.1038/s41467-019-11601-2>, 2019.
- Beck, H. E., Zimmermann, N. E., McVicar, T. R., Vergopolan, N., Berg, A., and Wood, E. F.: Present and future Köppen-Geiger climate classification maps at 1-km resolution, *Sci Data*, 5, 180214, <https://doi.org/10.1038/sdata.2018.214>, 2018.
- Bierman, P. R., Marsella, K. A., Patterson, C., Davis, P. T., and Caffee, M.: Mid-Pleistocene cosmogenic minimum-age limits for pre-Wisconsinan glacial surfaces in southwestern Minnesota and southern Baffin Island: a multiple nuclide approach, *Geomorphology*, 27, 25–39, [https://doi.org/10.1016/S0169-555X\(98\)00088-9](https://doi.org/10.1016/S0169-555X(98)00088-9), 1999.
- Bierman, P. R., Marsella, K. A., Davis, P. T., and Caffee, M. W.: Response to Discussion by Wolfe et al. on Bierman et al. (*Geomorphology* 25 (1999) 25–39), *Geomorphology*, 39, 255–260, [https://doi.org/10.1016/S0169-555X\(00\)00102-1](https://doi.org/10.1016/S0169-555X(00)00102-1), 2001.
- Bierman, P. R., Caffee, M. W., Davis, P. T., Marsella, K., Pavich, M., Colgan, P., Mickelson, D., and Larsen, J.: Rates and Timing of Earth Surface Processes From In Situ-Produced Cosmogenic Be-10, *Reviews in Mineralogy and Geochemistry*, 50, 147–205, <https://doi.org/10.2138/rmg.2002.50.4>, 2002.
- Bierman, P. R., Davis, P. T., Corbett, L. B., Lifton, N. A., and Finkel, R. C.: Cold-based Laurentide ice covered New England's highest summits during the Last Glacial Maximum, *Geology*, G37225.1, <https://doi.org/10.1130/G37225.1>, 2015.
- Bierman, P. R., Shakun, J. D., Corbett, L. B., Zimmerman, S. R., and Rood, D. H.: A persistent and dynamic East Greenland Ice Sheet over the past 7.5 million years, *Nature*, 540, 256–260, <https://doi.org/10.1038/nature20147>, 2016.
- Bierman, P. R., Mastro, H. M., Peteet, D. M., Corbett, L. B., Steig, E. J., Halsted, C. T., Caffee, M. M., Hidy, A. J., Balco, G., Bennike, O., and Rock, B.: Plant, insect, and fungi fossils under the center of Greenland's ice sheet are evidence of ice-free times, *Proc. Natl. Acad. Sci. U.S.A.*, 121, e2407465121, <https://doi.org/10.1073/pnas.2407465121>, 2024a.
- Bierman, P. R., Christ, A. J., Collins, C. M., Mastro, H. M., Souza, J., Blard, P.-H., Brachfeld, S., Courville, Z. R., Rittenour, T. M., Thomas, E. K., Tison, J.-L., and Fripiat, F.: Scientific history, sampling approach, and physical characterization of the Camp Century subglacial material, a rare archive from beneath the Greenland Ice Sheet, *The Cryosphere*, 18, 4029–4052, <https://doi.org/10.5194/tc-18-4029-2024>, 2024b.
- Blard, P.-H., Protin, M., Tison, J.-L., Fripiat, F., Dahl-Jensen, D., Steffensen, J. P., Mahaney, W. C., Bierman, P. R., Christ, A. J., Corbett, L. B., Debaille, V., Rigaudier, T., Claeys, P., and ASTER Team: Basal debris of the NEEM ice core, Greenland: a window into sub-ice-sheet geology, basal ice processes and ice-sheet oscillations, *J. Glaciol.*, 69, 1011–1029, <https://doi.org/10.1017/jog.2022.122>, 2023.
- Bond, G., Heinrich, H., Broecker, W., Labeyrie, L., McManus, J., Andrews, J., Huon, S., Jantschik, R., Clasen, S., Simet, C., Tedesco, K., Klas, M., Bonani, G., and Ivy, S.: Evidence for massive discharges of icebergs into the North Atlantic ocean during the last glacial period, *Nature*, 360, 245–249, <https://doi.org/10.1038/360245a0>, 1992.
- Booth, D. B.: Glaciofluvial infilling and scour of the Puget Lowland, Washington, during ice-sheet glaciation, *Geol*, 22, 695, [https://doi.org/10.1130/0091-7613\(1994\)022<0695:GIASOT>2.3.CO;2](https://doi.org/10.1130/0091-7613(1994)022<0695:GIASOT>2.3.CO;2), 1994.
- Braucher, R., Bourlès, D., Merchel, S., Vidal Romani, J., Fernandez-Mosquera, D., Marti, K., Léanni, L., Chauvet, F., Arnold, M., Aumaître, G., and Keddadouche, K.: Determination of muon attenuation lengths in depth profiles from

in situ produced cosmogenic nuclides, *Nuclear Instruments and Methods in Physics Research Section B: Beam Interactions with Materials and Atoms*, 294, 484–490, <https://doi.org/10.1016/j.nimb.2012.05.023>, 2013.

Braucher, R., Guillou, V., Bourlès, D. L., Arnold, M., Aumaître, G., Keddadouche, K., and Nottoli, E.: Preparation of ASTER in-house  $^{10}\text{Be}/^{9}\text{Be}$  standard solutions, *Nuclear Instruments and Methods in Physics Research Section B: Beam Interactions with Materials and Atoms*, 361, 335–340, <https://doi.org/10.1016/j.nimb.2015.06.012>, 2015.

Briner, J. P. and Swanson, T. W.: Using inherited cosmogenic  $^{36}\text{Cl}$  to constrain glacial erosion rates of the Cordilleran ice sheet, *Geol.*, 26, 3, [https://doi.org/10.1130/0091-7613\(1998\)026<0003:UICCTC>2.3.CO;2](https://doi.org/10.1130/0091-7613(1998)026<0003:UICCTC>2.3.CO;2), 1998.

Briner, J. P., Miller, G. H., Davis, P. T., and Finkel, R. C.: Cosmogenic radionuclides from fiord landscapes support differential erosion by overriding ice sheets, *Geological Society of America Bulletin*, 118, 406–420, <https://doi.org/10.1130/B25716.1>, 2006.

Briner, J. P., Goehring, B. M., Mangerud, J., and Svendsen, J. I.: The deep accumulation of  $^{10}\text{Be}$  at Utsira, southwestern Norway: Implications for cosmogenic nuclide exposure dating in peripheral ice sheet landscapes, *Geophysical Research Letters*, 43, 9121–9129, <https://doi.org/10.1002/2016GL070100>, 2016.

Carlson, A. E., Clark, P. U., Raisbeck, G. M., and Brook, E. J.: Rapid Holocene Deglaciation of the Labrador Sector of the Laurentide Ice Sheet, *Journal of Climate*, 20, 5126–5133, <https://doi.org/10.1175/JCLI4273.1>, 2007.

Christ, A. J., Bierman, P. R., Knutz, P. C., Corbett, L. B., Fosdick, J. C., Thomas, E. K., Cowling, O. C., Hidy, A. J., and Caffee, M. W.: The Northwestern Greenland Ice Sheet during the Early Pleistocene was similar to today, *Geophysical Research Letters*, 47, <https://doi.org/10.1029/2019GL085176>, 2020.

Christ, A. J., Bierman, P. R., Schaefer, J. M., Dahl-Jensen, D., Steffensen, J. P., Corbett, L. B., Peteet, D. M., Thomas, E. K., Steig, E. J., Rittenour, T. M., Tison, J.-L., Blard, P.-H., Perdrial, N., Dethier, D. P., Lini, A., Hidy, A. J., Caffee, M. W., and Southon, J.: A multimillion-year-old record of Greenland vegetation and glacial history preserved in sediment beneath 1.4 km of ice at Camp Century, *Proc. Natl. Acad. Sci. U.S.A.*, 118, e2021442118, <https://doi.org/10.1073/pnas.2021442118>, 2021.

Christ, A. J., Rittenour, T. M., Bierman, P. R., Keisling, B. A., Knutz, P. C., Thomsen, T. B., Keulen, N., Fosdick, J. C., Hemming, S. R., Tison, J.-L., Blard, P.-H., Steffensen, J. P., Caffee, M. W., Corbett, L. B., Dahl-Jensen, D., Dethier, D. P., Hidy, A. J., Perdrial, N., Peteet, D. M., Steig, E. J., and Thomas, E. K.: Deglaciation of northwestern Greenland during Marine Isotope Stage 11, *Science*, 381, 330–335, <https://doi.org/10.1126/science.ade4248>, 2023.

Clark, P. U., Brook, E. J., Raisbeck, G. M., Yiou, F., and Clark, J.: Cosmogenic  $^{10}\text{Be}$  ages of the Saglek Moraines, Torngat Mountains, Labrador, *Geol.*, 31, 617, [https://doi.org/10.1130/0091-7613\(2003\)031<0617:CBAOTS>2.0.CO;2](https://doi.org/10.1130/0091-7613(2003)031<0617:CBAOTS>2.0.CO;2), 2003.

Colgan, P. M., Bierman, P. R., Mickelson, D. M., and Caffee, M.: Variation in glacial erosion near the southern margin of the Laurentide Ice Sheet, south-central Wisconsin, USA: Implications for cosmogenic dating of glacial terrains, *Geological Society of America Bulletin*, 114, 1581–1591, [https://doi.org/10.1130/0016-7606\(2002\)114<1581:VIGENT>2.0.CO;2](https://doi.org/10.1130/0016-7606(2002)114<1581:VIGENT>2.0.CO;2), 2002.

Collins, C. M., Perdrial, N., Blard, P.-H., Keulen, N., Mahaney, W. C., Mastro, H., Souza, J., Rizzo, D. M., Marrocchi, Y., Knutz, P. C., and Bierman, P. R.: Characterization of the 1966 Camp Century Sub-Glacial Core: A Multiscale Analysis, *EGU sphere*, 1–33, <https://doi.org/10.5194/egusphere-2024-2194>, 2024.

Corbett, L. B., Young, N. E., Bierman, P. R., Briner, J. P., Neumann, T. A., Rood, D. H., and Graly, J. A.: Paired bedrock and boulder  $^{10}\text{Be}$  concentrations resulting from early Holocene ice retreat near Jakobshavn Isfjord, western Greenland, *Quaternary Science Reviews*, 30, 1739–1749, <https://doi.org/10.1016/j.quascirev.2011.04.001>, 2011.

Corbett, L. B., Bierman, P. R., and Rood, D. H.: An approach for optimizing in situ cosmogenic  $^{10}\text{Be}$  sample preparation, *Quaternary Geochronology*, 33, 24–34, <https://doi.org/10.1016/j.quageo.2016.02.001>, 2016a.

- Corbett, L. B., Bierman, P. R., and Rood, D. H.: Constraining multi-stage exposure-burial scenarios for boulders preserved beneath cold-based glacial ice in Thule, northwest Greenland, *Earth and Planetary Science Letters*, 440, 147–157, <https://doi.org/10.1016/j.epsl.2016.02.004>, 2016b.
- Corbett, L. B., Bierman, P. R., and Davis, P. T.: Glacial history and landscape evolution of southern Cumberland Peninsula, Baffin Island, Canada, constrained by cosmogenic<sup>10</sup>Be and<sup>26</sup>Al, *Geological Society of America Bulletin*, 128, 1173–1192, <https://doi.org/10.1130/B31402.1>, 2016c.
- Corbett, L. B., Bierman, P. R., Rood, D. H., Caffee, M. W., Lifton, N. A., and Woodruff, T. E.: Cosmogenic <sup>26</sup>Al/<sup>10</sup>Be surface production ratio in Greenland, *Geophysical Research Letters*, 44, 1350–1359, <https://doi.org/10.1002/2016GL071276>, 2017.
- Corbett, L. B., Bierman, P. R., Wright, S. F., Shakun, J. D., Davis, P. T., Goehring, B. M., Halsted, C. T., Koester, A. J., Caffee, M. W., and Zimmerman, S. R.: Analysis of multiple cosmogenic nuclides constrains Laurentide Ice Sheet history and process on Mt. Mansfield, Vermont’s highest peak, *Quaternary Science Reviews*, 205, 234–246, <https://doi.org/10.1016/j.quascirev.2018.12.014>, 2019.
- Corbett, L. B., Bierman, P. R., Neumann, T. A., Graly, J. A., Shakun, J. D., Goehring, B. M., Hidy, A. J., and Caffee, M. W.: Measuring multiple cosmogenic nuclides in glacial cobbles sheds light on Greenland Ice Sheet processes, *Earth and Planetary Science Letters*, 554, 116673, <https://doi.org/10.1016/j.epsl.2020.116673>, 2021.
- Couette, P., Ghienne, J., Lajeunesse, P., and Van Der Woerd, J.: Climatic control on the retreat of the Laurentide Ice Sheet margin in easternmost Québec–Labrador (Canada) revealed by cosmogenic nuclide exposure dating, *J Quaternary Science*, 38, 1044–1061, <https://doi.org/10.1002/jqs.3525>, 2023.
- Cowton, T., Nienow, P., Bartholomew, I., Sole, A., and Mair, D.: Rapid erosion beneath the Greenland ice sheet, *Geology*, 40, 343–346, <https://doi.org/10.1130/G32687.1>, 2012.
- Dalton, A. S., Finkelstein, S. A., Forman, S. L., Barnett, P. J., Pico, T., and Mitrovica, J. X.: Was the Laurentide Ice Sheet significantly reduced during Marine Isotope Stage 3?, *Geology*, 47, 111–114, <https://doi.org/10.1130/G45335.1>, 2019.
- Dalton, A. S., Margold, M., Stokes, C. R., Tarasov, L., Dyke, A. S., Adams, R. S., Allard, S., Arends, H. E., Atkinson, N., Attig, J. W., Barnett, P. J., Barnett, R. L., Batterson, M., Bernatchez, P., Borns, H. W., Breckenridge, A., Briner, J. P., Brouard, E., Campbell, J. E., Carlson, A. E., Clague, J. J., Curry, B. B., Daigneault, R.-A., Dubé-Loubert, H., Easterbrook, D. J., Franzi, D. A., Friedrich, H. G., Funder, S., Gauthier, M. S., Gowan, A. S., Harris, K. L., Héту, B., Hooyer, T. S., Jennings, C. E., Johnson, M. D., Kehew, A. E., Kelley, S. E., Kerr, D., King, E. L., Kjeldsen, K. K., Knaeble, A. R., Lajeunesse, P., Lakeman, T. R., Lamothe, M., Larson, P., Lavoie, M., Loope, H. M., Lowell, T. V., Lusardi, B. A., Manz, L., McMartin, I., Nixon, F. C., Occhietti, S., Parkhill, M. A., Piper, D. J. W., Pronk, A. G., Richard, P. J. H., Ridge, J. C., Ross, M., Roy, M., Seaman, A., Shaw, J., Stea, R. R., Teller, J. T., Thompson, W. B., Thorleifson, L. H., Utting, D. J., Veillette, J. J., Ward, B. C., Weddle, T. K., and Wright, H. E.: An updated radiocarbon-based ice margin chronology for the last deglaciation of the North American Ice Sheet Complex, *Quaternary Science Reviews*, 234, 106223, <https://doi.org/10.1016/j.quascirev.2020.106223>, 2020.
- Dalton, A. S., Stokes, C. R., and Batchelor, C. L.: Evolution of the Laurentide and Innuitian ice sheets prior to the Last Glacial Maximum (115 ka to 25 ka), *Earth-Science Reviews*, 224, 103875, <https://doi.org/10.1016/j.earscirev.2021.103875>, 2022.
- Dalton, A. S., Dulfer, H. E., Margold, M., Heyman, J., Clague, J. J., Froese, D. G., Gauthier, M. S., Hughes, A. L. C., Jennings, C. E., Norris, S. L., and Stoker, B. J.: Deglaciation of the North American ice sheet complex in calendar years based on a comprehensive database of chronological data: NADI-1, *Quaternary Science Reviews*, 321, 108345, <https://doi.org/10.1016/j.quascirev.2023.108345>, 2023.
- Davis, P. T., Bierman, P. R., Corbett, L. B., and Finkel, R. C.: Cosmogenic exposure age evidence for rapid Laurentide deglaciation of the Katahdin area, west-central Maine, USA, 16 to 15 ka, *Quaternary Science Reviews*, 116, 95–105, <https://doi.org/10.1016/j.quascirev.2015.03.021>, 2015.

Dethier, D. P., Racela, J., and Wieman, S. T.: A contemporary mass-balance approach to small-catchment denudation rates in glaciated New England, GSA Annual Meeting in Indianapolis, Indiana, USA - 2018, 319718, <https://doi.org/10.1130/abs/2018AM-319718>, 2018.

Dubé-Loubert, H., Roy, M., Schaefer, J. M., and Clark, P. U.:  $^{10}\text{Be}$  dating of former glacial Lake Naskaupi (Québec-Labrador) and timing of its discharges during the last deglaciation, *Quaternary Science Reviews*, 191, 31–40, <https://doi.org/10.1016/j.quascirev.2018.05.008>, 2018.

Dubé-Loubert, H., Roy, M., Veillette, J. J., Brouard, E., Schaefer, J. M., and Wittmann, H.: The role of glacial dynamics in the development of ice divides and the Horseshoe Intersection Zone of the northeastern Labrador Sector of the Laurentide Ice Sheet, *Geomorphology*, 387, 107777, <https://doi.org/10.1016/j.geomorph.2021.107777>, 2021.

Dyke, A. S.: An outline of North American deglaciation with emphasis on central and northern Canada, in: *Developments in Quaternary Sciences*, vol. 2, Elsevier, 373–424, [https://doi.org/10.1016/S1571-0866\(04\)80209-4](https://doi.org/10.1016/S1571-0866(04)80209-4), 2004.

Fame, M. L., Owen, L. A., Spotila, J. A., Dortch, J. M., and Caffee, M. W.: Tracking paraglacial sediment with cosmogenic  $^{10}\text{Be}$  using an example from the northwest Scottish Highlands, *Quaternary Science Reviews*, 182, 20–36, <https://doi.org/10.1016/j.quascirev.2017.12.017>, 2018.

Ganti, V., Von Hagke, C., Scherler, D., Lamb, M. P., Fischer, W. W., and Avouac, J.-P.: Time scale bias in erosion rates of glaciated landscapes, *Sci. Adv.*, 2, e1600204, <https://doi.org/10.1126/sciadv.1600204>, 2016.

Gauthier, M. S., Hodder, T. J., Dalton, A. S., Brewer, V., Lian, O. B., Finkelstein, S. A., Schaarschmidt, M., and Mereghetti, A.: South-central Laurentide Ice Sheet dynamics and the formation of proglacial Lake Vita during MIS 3, *Quat. res.*, 1–23, <https://doi.org/10.1017/qua.2024.34>, 2024.

Goehring, B. M., Kelly, M. A., Schaefer, J. M., Finkel, R. C., and Lowell, T. V.: Dating of raised marine and lacustrine deposits in east Greenland using beryllium-10 depth profiles and implications for estimates of subglacial erosion, *J Quaternary Science*, 25, 865–874, <https://doi.org/10.1002/jqs.1380>, 2010.

Goldthwait, J. W. and Kruger, F. C.: Weathered rock in and under the drift in New Hampshire, *Geological Society of America Bulletin*, 49, 1183–1198, <https://doi.org/10.1130/GSAB-49-1183>, 1938.

Granger, D. E.: Cosmogenic Nuclide Burial Dating in Archaeology and Paleoanthropology, in: *Treatise on Geochemistry*, Elsevier, 81–97, <https://doi.org/10.1016/B978-0-08-095975-7.01208-0>, 2014.

Granger, D. E. and Muzikar, P. F.: Dating sediment burial with in situ-produced cosmogenic nuclides: theory, techniques, and limitations, *Earth and Planetary Science Letters*, 188, 269–281, [https://doi.org/10.1016/S0012-821X\(01\)00309-0](https://doi.org/10.1016/S0012-821X(01)00309-0), 2001.

Hallet, B., Hunter, L., and Bogen, J.: Rates of erosion and sediment evacuation by glaciers: A review of field data and their implications, *Global and Planetary Change*, 12, 213–235, [https://doi.org/10.1016/0921-8181\(95\)00021-6](https://doi.org/10.1016/0921-8181(95)00021-6), 1996.

Halsted, C. T., Bierman, P. R., Shakun, J. D., Davis, P. T., Corbett, L. B., Drebber, J. S., and Ridge, J. C.: A critical re-analysis of constraints on the timing and rate of Laurentide Ice Sheet recession in the northeastern United States, *J Quaternary Science*, 39, 54–69, <https://doi.org/10.1002/jqs.3563>, 2024.

Heisinger, B., Lal, D., Jull, A. J. T., Kubik, P., Ivy-Ochs, S., Knie, K., and Nolte, E.: Production of selected cosmogenic radionuclides by muons: 2. Capture of negative muons, *Earth and Planetary Science Letters*, 200, 357–369, [https://doi.org/10.1016/S0012-821X\(02\)00641-6](https://doi.org/10.1016/S0012-821X(02)00641-6), 2002.

Heyman, J., Stroeven, A. P., Harbor, J. M., and Caffee, M. W.: Too young or too old: Evaluating cosmogenic exposure dating based on an analysis of compiled boulder exposure ages, *Earth and Planetary Science Letters*, 302, 71–80, <https://doi.org/10.1016/j.epsl.2010.11.040>, 2011.

- Hildes, D. H. D., Clarke, G. K. C., Flowers, G. E., and Marshall, S. J.: Subglacial erosion and englacial sediment transport modelled for North American ice sheets, *Quaternary Science Reviews*, 23, 409–430, <https://doi.org/10.1016/j.quascirev.2003.06.005>, 2004.
- Hodder, T. J., Gauthier, M. S., Ross, M., and Lian, O. B.: Was there a nonglacial episode in the western Hudson Bay Lowland during Marine Isotope Stage 3?, *Quat. res.*, 116, 148–161, <https://doi.org/10.1017/qua.2023.35>, 2023.
- Hodder, T. J., Gauthier, M. S., Ross, M., Kelley, S. E., Lian, O. B., Dalton, A. S., and Finkelstein, S. A.: Unravelling the fragmented sediment–landform assemblage in an area of thick Quaternary sediment, western Hudson Bay Lowland, Canada, *Can. J. Earth Sci.*, 61, 1156–1183, <https://doi.org/10.1139/cjes-2024-0018>, 2024.
- Hynes, A. and Rivers, T.: Protracted continental collision — evidence from the Grenville Orogen *Lithoprobe — parameters, processes, and the evolution of a continent*., *Can. J. Earth Sci.*, 47, 591–620, <https://doi.org/10.1139/E10-003>, 2010.
- Jones, R. S., Whitehouse, P. L., Bentley, M. J., Small, D., and Dalton, A. S.: Impact of glacial isostatic adjustment on cosmogenic surface-exposure dating, *Quaternary Science Reviews*, 212, 206–212, <https://doi.org/10.1016/j.quascirev.2019.03.012>, 2019.
- Klein, J., Giegengack, R., Middleton, R., Sharma, P., Underwood, J. R., and Weeks, R. A.: Revealing Histories of Exposure Using *In Situ* Produced  $^{26}\text{Al}$  and  $^{10}\text{Be}$  in Libyan Desert Glass, *Radiocarbon*, 28, 547–555, <https://doi.org/10.1017/S0033822200007700>, 1986.
- Koester, A. J., Shakun, J. D., Bierman, P. R., Davis, P. T., Corbett, L. B., Goehring, B. M., Vickers, A. C., and Zimmerman, S. R.: Laurentide ice sheet thinning and erosive regimes at Mount Washington, New Hampshire, inferred from multiple cosmogenic nuclides, in: *Untangling the Quaternary Period—A Legacy of Stephen C. Porter*, edited by: Waitt, R. B., Thackray, G. D., and Gillespie, A. R., Geological Society of America, 299–314, [https://doi.org/10.1130/2020.2548\(15\)](https://doi.org/10.1130/2020.2548(15)), 2021.
- Kohl, C. P. and Nishiizumi, K.: Chemical isolation of quartz for measurement of in-situ -produced cosmogenic nuclides, *Geochimica et Cosmochimica Acta*, 56, 3583–3587, [https://doi.org/10.1016/0016-7037\(92\)90401-4](https://doi.org/10.1016/0016-7037(92)90401-4), 1992.
- Koppes, M., Hallet, B., Rignot, E., Mouginit, J., Wellner, J. S., and Boldt, K.: Observed latitudinal variations in erosion as a function of glacier dynamics, *Nature*, 526, 100–103, <https://doi.org/10.1038/nature15385>, 2015.
- Lajeunesse, P. and Allard, M.: Late Quaternary Deglaciation, Glaciomarine Sedimentation and Glacioisostatic Recovery in the Rivière Nastapoka Area, Eastern Hudson Bay, Northern Québec, *Géographie physique et Quaternaire*, 57, 65–83, <https://doi.org/10.7202/010331ar>, 2005.
- Larue, F., Royer, A., De Sève, D., Langlois, A., Roy, A., and Brucker, L.: Validation of GlobSnow-2 snow water equivalent over Eastern Canada, *Remote Sensing of Environment*, 194, 264–277, <https://doi.org/10.1016/j.rse.2017.03.027>, 2017.
- LaSalle, P., De Kimpe, C. R., and Laverdiere, M. R.: Sub-till saprolites in southeastern Quebec and adjacent New England: Erosional, stratigraphic, and climatic significance, in: *Geological Society of America Special Papers*, vol. 197, Geological Society of America, 13–20, <https://doi.org/10.1130/SPE197-p13>, 1985.
- Lavoie, C., Allard, M., and Duhamel, D.: Deglaciation landforms and C-14 chronology of the Lac Guillaume-Delisle area, eastern Hudson Bay: A report on field evidence, *Geomorphology*, 159–160, 142–155, <https://doi.org/10.1016/j.geomorph.2012.03.015>, 2012.
- LeBlanc, D. E., Shakun, J. D., Corbett, L. B., Bierman, P. R., Caffee, M. W., and Hidy, A. J.: Laurentide Ice Sheet persistence during Pleistocene interglacials, *Geology*, 51, 496–499, <https://doi.org/10.1130/G50820.1>, 2023.
- Lefebvre-Fortier, C., Roy, M., Dubé-Loubert, H., Brouard, E., and Schaefer, J. M.: Configuration and timing of the postglacial marine incursion along the eastern Ungava Peninsula (Nunavik, Canada): implications for deglaciation models, *J Quaternary Science*, 39, 359–372, <https://doi.org/10.1002/jqs.3591>, 2024.

- Lifton, N., Sato, T., and Dunai, T. J.: Scaling in situ cosmogenic nuclide production rates using analytical approximations to atmospheric cosmic-ray fluxes, *Earth and Planetary Science Letters*, 386, 149–160, <https://doi.org/10.1016/j.epsl.2013.10.052>, 2014.
- Liverman, D. G. E.: Quaternary geology of the Goose Bay area., Current Research. Department of Mines and Energy, Geological Survey, Newfoundland and Labrador, Report, 1997.
- Marquette, G. C., Gray, J. T., Gosse, J. C., Courchesne, F., Stockli, L., Macpherson, G., and Finkel, R.: Felsenmeer persistence under non-erosive ice in the Torngat and Kaumajet mountains, Quebec and Labrador, as determined by soil weathering and cosmogenic nuclide exposure dating, *Can. J. Earth Sci.*, 41, 19–38, <https://doi.org/10.1139/e03-072>, 2004.
- Marsella, K. A., Bierman, P. R., Davis, P. T., and Caffee, M. W.: Cosmogenic  $^{10}\text{Be}$  and  $^{26}\text{Al}$  ages for the Last Glacial Maximum, eastern Baffin Island, Arctic Canada, *Geological Society of America Bulletin*, 112, 1296–1312, [https://doi.org/10.1130/0016-7606\(2000\)112<1296:CBAAAF>2.0.CO;2](https://doi.org/10.1130/0016-7606(2000)112<1296:CBAAAF>2.0.CO;2), 2000.
- Melanson, A., Bell, T., and Tarasov, L.: Numerical modelling of subglacial erosion and sediment transport and its application to the North American ice sheets over the Last Glacial cycle, *Quaternary Science Reviews*, 68, 154–174, <https://doi.org/10.1016/j.quascirev.2013.02.017>, 2013.
- Merchel, S. and Bremser, W.: First international  $^{26}\text{Al}$  interlaboratory comparison – Part I, *Nuclear Instruments and Methods in Physics Research Section B: Beam Interactions with Materials and Atoms*, 223–224, 393–400, <https://doi.org/10.1016/j.nimb.2004.04.076>, 2004.
- Miller, G., Briner, J., Lifton, N., and Finkel, R.: Limited ice-sheet erosion and complex exposure histories derived from in situ cosmogenic  $^{10}\text{Be}$ ,  $^{26}\text{Al}$ , and  $^{14}\text{C}$  on Baffin Island, Arctic Canada, *Quaternary Geochronology*, 1, 74–85, <https://doi.org/10.1016/j.quageo.2006.06.011>, 2006.
- Miller, G. H. and Andrews, J. T.: Hudson Bay was not deglaciated during MIS-3, *Quaternary Science Reviews*, 225, 105944, <https://doi.org/10.1016/j.quascirev.2019.105944>, 2019.
- Nelson, A. H., Bierman, P. R., Shakun, J. D., and Rood, D. H.: Using *in situ* cosmogenic  $^{10}\text{Be}$  to identify the source of sediment leaving Greenland, *Earth Surf. Process. Landforms*, 39, 1087–1100, <https://doi.org/10.1002/esp.3565>, 2014.
- Nishiizumi, K.: Preparation of  $^{26}\text{Al}$  AMS standards, *Nuclear Instruments and Methods in Physics Research Section B: Beam Interactions with Materials and Atoms*, 223–224, 388–392, <https://doi.org/10.1016/j.nimb.2004.04.075>, 2004.
- Nishiizumi, K., Imamura, M., Caffee, M. W., Southon, J. R., Finkel, R. C., and McAninch, J.: Absolute calibration of  $^{10}\text{Be}$  AMS standards, *Nuclear Instruments and Methods in Physics Research Section B: Beam Interactions with Materials and Atoms*, 258, 403–413, <https://doi.org/10.1016/j.nimb.2007.01.297>, 2007.
- Occhietti, S., Parent, M., Lajeunesse, P., Robert, F., and Govare, É.: Late Pleistocene–Early Holocene Decay of the Laurentide Ice Sheet in Québec–Labrador, in: *Developments in Quaternary Sciences*, vol. 15, Elsevier, 601–630, <https://doi.org/10.1016/B978-0-444-53447-7.00047-7>, 2011.
- Patton, H., Hubbard, A., Heyman, J., Alexandropoulou, N., Lasabuda, A. P. E., Stroeven, A. P., Hall, A. M., Winsborrow, M., Sugden, D. E., Kleman, J., and Andreassen, K.: The extreme yet transient nature of glacial erosion, *Nat Commun*, 13, 7377, <https://doi.org/10.1038/s41467-022-35072-0>, 2022.
- Patton, H., Alexandropoulou, N., Lasabuda, A. P. E., Knies, J., Andreassen, K., Winsborrow, M., Laberg, J. S., and Hubbard, A.: Glacial erosion and Quaternary landscape development of the Eurasian Arctic, *Earth-Science Reviews*, 258, 104936, <https://doi.org/10.1016/j.earscirev.2024.104936>, 2024.
- Payette, S., Morneau, C., Sirois, L., and Despons, M.: Recent Fire History of the Northern Quebec Biomes, *Ecology*, 70, 656–673, <https://doi.org/10.2307/1940217>, 1989.

Pelletier, J. D., Broxton, P. D., Hazenbarg, P., Zenf, X., Troch, P. A., Niu, G., Williams, Z. C., Brunke, M. A., and Gochis, D.: Global 1-km Gridded Thickness of Soil, Regolith, and Sedimentary Deposit Layers, <https://doi.org/10.3334/ORNDAAC/1304>, 2016.

Peteet, D. M., Beh, M., Orr, C., Kurdyla, D., Nichols, J., and Guilderson, T.: Delayed deglaciation or extreme Arctic conditions 21–16 cal. kyr at southeastern Laurentide Ice Sheet margin?, *Geophysical Research Letters*, 39, 2012GL051884, <https://doi.org/10.1029/2012GL051884>, 2012.

Pico, T., Birch, L., Weisenberg, J., and Mitrovica, J. X.: Refining the Laurentide Ice Sheet at Marine Isotope Stage 3: A data-based approach combining glacial isostatic simulations with a dynamic ice model, *Quaternary Science Reviews*, 195, 171–179, <https://doi.org/10.1016/j.quascirev.2018.07.023>, 2018.

Rice, J. M., Ross, M., Paulen, R. C., Kelley, S. E., Briner, J. P., Neudorf, C. M., and Lian, O. B.: Refining the ice flow chronology and subglacial dynamics across the migrating Labrador Divide of the Laurentide Ice Sheet with age constraints on deglaciation, *J Quaternary Science*, 34, 519–535, <https://doi.org/10.1002/jqs.3138>, 2019.

Schaefer, J. M., Finkel, R. C., Balco, G., Alley, R. B., Caffee, M. W., Briner, J. P., Young, N. E., Gow, A. J., and Schwartz, R.: Greenland was nearly ice-free for extended periods during the Pleistocene, *Nature*, 540, 252–255, <https://doi.org/10.1038/nature20146>, 2016.

Schildgen, T. F., Phillips, W. M., and Purves, R. S.: Simulation of snow shielding corrections for cosmogenic nuclide surface exposure studies, *Geomorphology*, 64, 67–85, <https://doi.org/10.1016/j.geomorph.2004.05.003>, 2005.

Shakun, J. D., Corbett, L. B., Bierman, P. R., Underwood, K., Rizzo, D. M., Zimmerman, S. R., Caffee, M. W., Naish, T., Golledge, N. R., and Hay, C. C.: Minimal East Antarctic Ice Sheet retreat onto land during the past eight million years, *Nature*, 558, 284–287, <https://doi.org/10.1038/s41586-018-0155-6>, 2018.

Simms, A. R., Lisiecki, L., Gebbie, G., Whitehouse, P. L., and Clark, J. F.: Balancing the last glacial maximum (LGM) sea-level budget, *Quaternary Science Reviews*, 205, 143–153, <https://doi.org/10.1016/j.quascirev.2018.12.018>, 2019.

Spray, J. G., Kelley, S. P., and Rowley, D. B.: Evidence for a late Triassic multiple impact event on Earth, *Nature*, 392, 171–173, <https://doi.org/10.1038/32397>, 1998.

Staiger, J., Gosse, J., Little, E., Utting, D., Finkel, R., Johnson, J., and Fastook, J.: Glacial erosion and sediment dispersion from detrital cosmogenic nuclide analyses of till, *Quaternary Geochronology*, 1, 29–42, <https://doi.org/10.1016/j.quageo.2006.06.009>, 2006.

Staiger, J. K. W., Gosse, J. C., Johnson, J. V., Fastook, J., Gray, J. T., Stockli, D. F., Stockli, L., and Finkel, R.: Quaternary relief generation by polythermal glacier ice, *Earth Surf Processes Landf*, 30, 1145–1159, <https://doi.org/10.1002/esp.1267>, 2005.

Stokes, C. R., Tarasov, L., and Dyke, A. S.: Dynamics of the North American Ice Sheet Complex during its inception and build-up to the Last Glacial Maximum, *Quaternary Science Reviews*, 50, 86–104, <https://doi.org/10.1016/j.quascirev.2012.07.009>, 2012.

Storrar, R. D., Stokes, C. R., and Evans, D. J. A.: A map of large Canadian eskers from Landsat satellite imagery, *Journal of Maps*, 9, 456–473, <https://doi.org/10.1080/17445647.2013.815591>, 2013.

Stroeven, A. P., Fabel, D., Harbor, J., Hättetstrand, C., and Kleman, J.: Quantifying the erosional impact of the Fennoscandian Ice Sheet in the Torneträsk–Narvik corridor, northern Sweden, based on cosmogenic radionuclide data, *Geografiska Annaler: Series A, Physical Geography*, 84, 275–287, <https://doi.org/10.1111/j.0435-3676.2002.00182.x>, 2002.

Sugden, D. E.: Glacial Erosion by the Laurentide Ice Sheet, *J. Glaciol.*, 20, 367–391, <https://doi.org/10.3189/S0022143000013915>, 1978.

Tiffney, B. H.: Re-evaluation of the age of the Brandon Lignite (Vermont, USA) based on plant megafossils, *Review of Palaeobotany and Palynology*, 82, 299–315, [https://doi.org/10.1016/0034-6667\(94\)90081-7](https://doi.org/10.1016/0034-6667(94)90081-7), 1994.

Ullman, D. J., Carlson, A. E., Hostetler, S. W., Clark, P. U., Cuzzone, J., Milne, G. A., Winsor, K., and Caffee, M.: Final Laurentide ice-sheet deglaciation and Holocene climate-sea level change, *Quaternary Science Reviews*, 152, 49–59, <https://doi.org/10.1016/j.quascirev.2016.09.014>, 2016.

Wilner, J. A., Nordin, B. J., Getraer, A., Gregoire, R. M., Krishna, M., Li, J., Pickell, D. J., Rogers, E. R., McDannell, K. T., Palucis, M. C., and Keller, C.: Limits to timescale dependence in erosion rates: Quantifying glacial and fluvial erosion across timescales, *Sci. Adv.*, 10, eadr2009, <https://doi.org/10.1126/sciadv.adr2009>, 2024.